Technical Report

TR-2009-012

Hierarchical Local Model Reduction for Elliptic Problems I: A Domain Decomposition Approach

by

S. Perotto, A. Ern, A. Veneziani

Mathematics and Computer Science

EMORY UNIVERSITY

HIERARCHICAL LOCAL MODEL REDUCTION FOR ELLIPTIC PROBLEMS I: A DOMAIN DECOMPOSITION APPROACH

SIMONA PEROTTO[§], ALEXANDRE ERN[†], AND ALESSANDRO VENEZIANI[‡]

Abstract. Some engineering applications, for instance related to fluid dynamics in pipe or channel networks, feature a dominant spatial direction along which the most relevant dynamics develop. Nevertheless, local features of the problem depending on the other directions, that we call *transverse*, can be locally relevant to the whole problem. We propose in the context of elliptic problems such as advection–diffusion–reaction equations, a hierarchical model reduction approach in which a coarse model featuring only the dominant direction dynamics is enriched locally by a fine model that accounts for the transverse variables via an appropriate modal expansion. We introduce a domain decomposition approach allowing us to employ a different number of modal functions in different parts of the domain according to the local complexity of the problem at hand. The methodology is investigated numerically on several test cases.

Key words. model reduction, domain decomposition method, modal expansion, finite elements

AMS subject classifications. 65N30, 65T40

1. Introduction and motivations. Many engineering applications exhibit a dominant direction that introduces an anisotropy in the most salient features of the problem. For instance, river dynamics, blood flow problems or air dynamics in internal combustion engines exhibit a main direction represented by the river bed, the vascular axial direction or the engine pipes.

For the sake of computational efficiency, it is sometimes possible in these cases to resort to *downscaled models* where only the dominant space dependence is considered. In haemodynamics, 1D models based on the Euler equations are used quite often (see, e.g., [11, Chap. 10]). Likewise in river hydrodynamics the flow can be generally modeled by the 1D shallow water equations (see, e.g., [24]). Nevertheless the simplifying assumptions at the basis of these downscaled models can *locally* fail, whenever the transverse dynamics become relevant. This could be due to a local reduction (stenosis) or enlargement (aneurysm) of a blood vessel, to the presence of an air-box in a combustion engine or to a bridge or a lake along a channel or a river network, respectively (see Figure 1.1, top for an example in the last framework). As a consequence, one would like to locally enhance the 1D approximation via a suitable higher-dimensional correction. A possible solution is the so-called *geometrical multiscale approach* (see, e.g., [10, 18, 15] and [11, Chap. 11]), where the downscaled model is locally replaced by a full 3D or 2D one (see Figure 1.1, middle).

Here we undertake a different methodology, referred to as *hierarchical model reduction* following the pioneering works of Babuška and Vogelius [21, 22] which address a different context, namely heat conduction in plates and shells. In the present paper, the problem at hand (the so-called *full model*) is reformulated by tackling in a different manner the dependence of the solution on the dominant direction and on the transverse ones. The former is spanned by a classical 1D piecewise polynomial basis of a finite element space. The latter are expanded into a *modal basis*. The

[†]Université Paris-Est, CERMICS, Ecole des Ponts, 6 et 8, av. Blaise Pascal, 77455 Marne la Vallée Cedex 2, France (ern@cermics.enpc.fr).

[§]MOX–Modeling and Scientific Computing, Dipartimento di Matematica "F. Brioschi", Politecnico di Milano, Via Bonardi 9, I-20133 Milano, Italy (simona.perotto@polimi.it).

[‡]Department of Mathematics and Computer Science, Emory University, Atlanta (GA), USA (ale@mathcs.emory.edu).

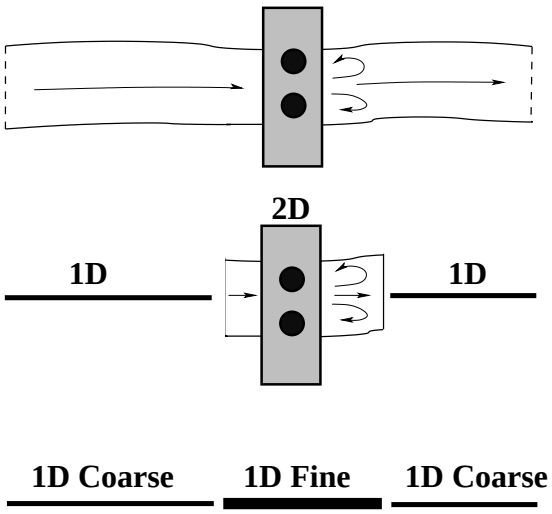

FIG. 1.1. *Full 2D representation of a channel with a bridge (top); geometrical multiscale reduction (middle); hierarchical model reduction (bottom).*

number of included modes determines the accuracy of the adopted model, according to the complexity of transverse dynamics (see Figure 1.1, bottom). We end up with a *hierarchy* of problems (the *reduced models*) that, in principle, can be tuned arbitrarily close to the full one.

The main feature of the present work is to address the situation where the level of model reduction can vary locally in the computational domain. This raises the issue of properly enforcing the matching conditions between adjacent subdomains. Similarly to what is done in the geometrical multiscale approach, we introduce a domain decomposition scheme to impose the matching between the areas characterized by different modal bases. This local reduction procedure is clearly advantageous from a computational viewpoint, whenever the full solution exhibits localized dynamics along the transverse directions. Indeed, our approach leads to solving a system of coupled problems, which are 1D, in contrast to the geometrical multiscale approach where problems with different dimensions (1D with 2D or 3D) are solved. The system dimension depends on the number of modal functions. In particular this work focuses on elliptic problems, e.g., advection–diffusion–reaction problems in pipe or channel networks (for an example of global model reduction in hydrodynamics we refer to [2]). Hierarchical local model reduction also paves the way to a model adaptation procedure which automatically detects the local level of model refinement to equilibrate, for instance, modeling and discretization errors. This will constitute the subject of the second part of this work ([16]).

This paper is organized as follows. In section 2 we describe the reference framework: we introduce the differential problem of interest and select a particular kind of computational domains, suited to the hierarchical model reduction we have in mind. Section 3 focuses on the simplified setting of global model reduction, by extending the preliminary analysis carried out in [9]. We define the reduced space and the reduced discrete formulation and we present numerical experiments. The local model reduc-

tion is carried out in section 4. We describe the domain decomposition scheme used to couple the local models with a different level of accuracy. Then, the methodology is assessed numerically. Some conclusions are drawn in the last section.

2. The setting. Let us introduce the weak form of the general elliptic problem to be approximated

$$\text{find } u \in V \quad : \quad a(u,v) = \mathcal{F}(v) \quad \forall v \in V, \tag{2.1}$$

with $a(\cdot,\cdot)$ and $\mathcal{F}(\cdot)$ a bilinear and a linear form, respectively, and V a Hilbert space. Boundary conditions are discussed below. Since we are interested in second-order elliptic problems, we assume that $V \subseteq H^1(\Omega)$. Standard notation for the Sobolev spaces, as well as for the spaces of functions bounded a.e. in Ω, is adopted. In the sequel, we denote with $\|\cdot\|_V := \|\cdot\|_{H^1(\Omega)}$ the norm associated with the space V, while $|\omega|$ stands for the measure of a generic (1D, 2D or 3D) set ω.
Suitable assumptions are made on the problem data to guarantee continuity and coercivity of $a(\cdot,\cdot)$ on V and continuity of $\mathcal{F}(\cdot)$ as well. Lax-Milgram Lemma ensures well-posedness of problem (2.1). Hereafter, we refer to (2.1) as to the *full problem*.

We assume Ω to coincide with the d-dimensional *fiber bundle*

$$\Omega = \bigcup_{x \in \Omega_{1D}} \{x\} \times \gamma_x,$$

where Ω_{1D} is a (supporting) one-dimensional domain, while $\gamma_x \subset \mathbb{R}^{d-1}$ represents the $(d-1)$-dimensional (transverse) *fiber* associated with the generic point $x \in \Omega_{1D}$. Thus we distinguish in Ω a *leading direction*, represented by Ω_{1D}, and a set of secondary orthogonal *transverse directions*, associated with the fibers γ_x. This approach differs with respect to the setting used in [21, 22, 23, 1, 3] where 1D models are associated with the transverse directions while the supporting fiber has dimension $(d-1)$.

For the sake of simplicity, we assume $\Omega_{1D} =]x_0, x_1[$ (see Figure 2.1). The more general case of a curved supporting fiber can also be considered. For any $x \in \Omega_{1D}$, let us introduce the map

$$\psi_x : \gamma_x \to \widehat{\gamma}_{d-1} \tag{2.2}$$

between the generic fiber γ_x and a reference fiber $\widehat{\gamma}_{d-1}$ of the same dimension. The notation $\mathbf{z} = (x, \mathbf{y})$ and $\widehat{\mathbf{z}} = (x, \widehat{\mathbf{y}})$ is adopted to denote a generic point in Ω and the corresponding point in $\widehat{\Omega}$, respectively via the map $\Psi : \Omega \to \widehat{\Omega}$, where $x \in \Omega_{1D}$ and $\widehat{\mathbf{y}} = \psi_x(\mathbf{y})$ with $\mathbf{y} \in \gamma_x$. The role played by Ψ is to map the current domain Ω into a reference domain $\widehat{\Omega} = \Omega_{1D} \times \widehat{\gamma}_{d-1}$ where the computations are easier and carried out once and for all (see Figure 2.1). Without loss of generality, we assume that $x \in \Omega_{1D}$ if and only if $(x, \mathbf{0}) \in \Omega$. In 2D, it is often possible to take for the map ψ_x in (2.2) the *linear transformation* defined by

$$\widehat{y} = \psi_x(y) = \frac{1}{L(x)} y, \tag{2.3}$$

where $L(x) = |\gamma_x|$ denotes the length of the fiber γ_x. In 3D the choice (2.3) is also possible in some situations, for instance when Ω is a cylindrical domain (see Figure 2.1, bottom). To discuss boundary conditions, let us partition the boundary of Ω into three disjoint sets Γ_0, Γ_1, and Γ_* such that

$$\Gamma_0 = \{x_0\} \times \gamma_{x_0}, \qquad \Gamma_1 = \{x_1\} \times \gamma_{x_1}, \qquad \Gamma_* = \bigcup_{x \in \Omega_{1D}} \{x\} \times \partial\gamma_x. \tag{2.4}$$

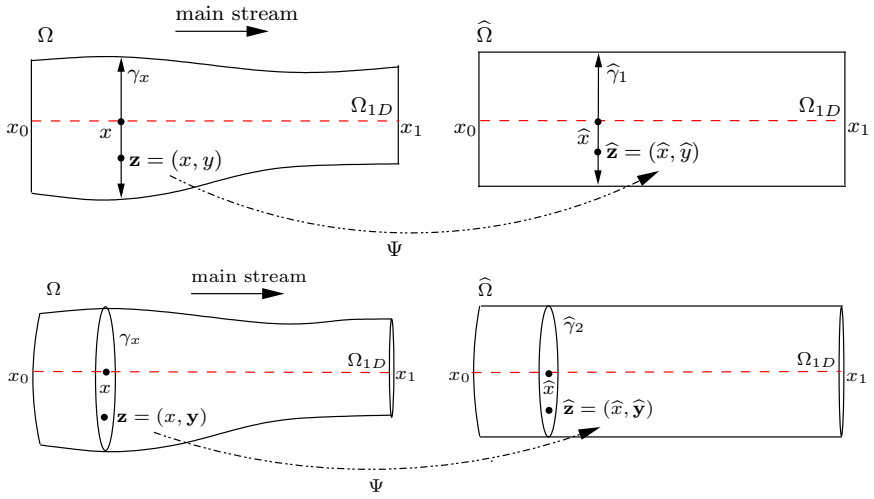

FIG. 2.1. *Examples of the map* Ψ *in* (2.2)*: the* 2D (*top*) *and the* 3D (*bottom*) *setting.*

On each of these three sets either homogeneous Dirichlet or Neumann boundary conditions are enforced. It is also possible to assign non-homogeneous Dirichlet data on Γ_0 and on Γ_1 (see Remark 1 below for a further discussion).

In the sequel, we assume that for all $x \in \Omega_{1D}$, ψ_x is a C^1-diffeomorphism. We also assume that the transformation Ψ is differentiable with respect to $\mathbf{z}$. This second assumption amounts to a smoothness hypothesis on Γ_*, i.e., Γ_* cannot have kinks. We denote with

$$\mathcal{J}(\mathbf{z}) = \frac{\partial \Psi}{\partial \mathbf{z}} = \begin{bmatrix} 1 & 0 \\ \dfrac{\partial \psi_x}{\partial x} & \nabla_{\mathbf{y}} \psi_x \end{bmatrix} \in \mathbb{R}^{d \times d}$$

the Jacobian associated with the map Ψ, where $\nabla_{\mathbf{y}}$ stands for the gradient with respect to $\mathbf{y}$. The first row is the same as in the identity matrix since the map Ψ does not modify the supporting fiber Ω_{1D}. In particular, we introduce the notation

$$\mathcal{D}_1(\mathbf{z}) = \frac{\partial \psi_x}{\partial x} \in \mathbb{R}^{d-1}, \qquad \mathcal{D}_2(\mathbf{z}) = \nabla_{\mathbf{y}} \psi_x \in \mathbb{R}^{(d-1)\times(d-1)}.$$

In the 2D case with the linear map (2.3), there holds

$$\mathcal{D}_1(\mathbf{z}) = -\frac{L'(x)}{L^2(x)} y, \qquad \mathcal{D}_2(\mathbf{z}) = \frac{1}{L(x)}.$$

In general (both 2D and 3D cases), via the Jacobian matrix $\mathcal{J}$, all the integrals on Ω can be reduced to integrals on the reference domain $\widehat{\Omega}$, since

$$\int_{\Omega} f(x, \mathbf{y})\, d\mathbf{z} = \int_{\widehat{\Omega}} f\big(x, \psi_x^{-1}(\widehat{\mathbf{y}})\big) \left| \det\big(\mathcal{D}_2^{-1}\big(x, \psi_x^{-1}(\widehat{\mathbf{y}})\big)\big)\right| d\widehat{\mathbf{z}}, \tag{2.5}$$

where $\mathcal{D}_2^{-1}$ is the so-called *deformation gradient tensor*.

3. Global model reduction. This section provides the formulation and the approximation of the reduced problem in the simplest situation of a global model reduction, that is, when the same number of modal functions is used along the transverse directions, uniformly on Ω_{1D}. Numerical results are also presented to assess the methodology.

3.1. Formulation of the globally reduced problem. We approximate problem (2.1) by exploiting the fiber structure introduced on Ω. We consider accordingly two basic components:

1. a space V_{1D} spanned by functions defined on the one-dimensional domain Ω_{1D}. In the present context of second-order elliptic problems, $V_{1D} \subseteq H^1(\Omega_{1D})$. The choice for the space V_{1D} must be compatible with the boundary conditions enforced on Γ_0 and on Γ_1; for instance, if a homogeneous Dirichlet boundary condition is assigned on Γ_0, functions in V_{1D} vanish at x_0;
2. a *modal basis* of functions $\{\varphi_k\}_{k\in\mathbb{N}^*} \in H^1(\widehat{\gamma}_{d-1})$, orthonormal with respect to the L^2-scalar product on $\widehat{\gamma}_{d-1}$, i.e., such that

$$\int_{\widehat{\gamma}_{d-1}} \varphi_k(\widehat{\mathbf{y}})\,\varphi_l(\widehat{\mathbf{y}})\,d\widehat{\mathbf{y}} = \delta_{kl} \quad \forall k,l \in \mathbb{N}^*, \tag{3.1}$$

with δ_{kl} the Kronecker symbol. Different choices are possible for the modal basis $\{\varphi_k\}_k$. We can use trigonometric functions (associated with Fourier expansions), Legendre polynomials, or wavelets, the index k having different meanings accordingly. If a homogeneous Dirichlet boundary condition is enforced on Γ_*, the modal basis functions must vanish on the boundary of $\widehat{\gamma}_{d-1}$.

By combining the space V_{1D} with the modal basis $\{\varphi_k\}_k$, we define the *reduced space*

$$V_m = \left\{ v_m(x,\mathbf{y}) = \sum_{k=1}^{m} \widetilde{v}_k(x)\,\varphi_k(\psi_x(\mathbf{y})),\ \text{with } \widetilde{v}_k \in V_{1D},\ x \in \Omega_{1D},\ \mathbf{y} \in \gamma_x \right\}, \tag{3.2}$$

where $m \in \mathbb{N}^*$ is a given integer, fixed a priori. Owing to the orthonormality condition (3.1), the frequency coefficients $\widetilde{v}_k$ in (3.2) are identified by the relation

$$\widetilde{v}_k(x) = \int_{\widehat{\gamma}_{d-1}} v_m\big(x, \psi_x^{-1}(\widehat{\mathbf{y}})\big)\,\varphi_k(\widehat{\mathbf{y}})\,d\widehat{\mathbf{y}} \quad \text{with } k = 1,\dots,m. \tag{3.3}$$

To obtain a well-defined and convergent approximation to the full problem (2.1), two properties of the space V_m in (3.2) are required:

i) *conformity* hypothesis: $V_m \subset V$, $\forall m \in \mathbb{N}^*$;

ii) *spectral approximability* hypothesis:

$$\forall\ v \in V \qquad \lim_{m\to+\infty} \Big(\inf_{v_m \in V_m} \|v - v_m\|_V \Big) = 0.$$

The so-called *reduced problem* reads: for any $m \in \mathbb{N}^*$,

$$\text{find } u_m \in V_m \quad : \quad a(u_m, v_m) = \mathcal{F}(v_m) \quad \forall v_m \in V_m. \tag{3.4}$$

The well-posedness of the formulation (3.4) immediately stems from the conformity hypothesis *i*) and the well-posedness assumed on (2.1). Moreover, because of the

conformity hypothesis *i*), the *modeling error* $e_m \in V$ given by the difference $u - u_m$ satisfies the *modeling orthogonality* property

$$a(e_m, v_m) = 0 \quad \forall v_m \in V_m. \tag{3.5}$$

Relation (3.5) readily leads to the *spectral optimality* property

$$\|e_m\|_V \leq C \inf_{v_m \in V_m} \|u - v_m\|_V,$$

where C depends on both the continuity and the coercivity constants of $a(\cdot,\cdot)$. Convergence of u_m to u thus follows from the spectral approximability hypothesis *ii*). Consequently, the modeling error can be controlled by suitably *tuning* the modal index m in the reduced formulation (3.4).

Exploiting in (3.4) the modal representation $u_m(\mathbf{z}) = \sum_{j=1}^m \widetilde{u}_j(x)\,\varphi_j(\psi_x(\mathbf{y})) \in V_m$ yields

$$\sum_{j=1}^{m} a(\widetilde{u}_j\varphi_j, \vartheta\varphi_k) = \mathcal{F}(\vartheta\varphi_k) \tag{3.6}$$

for any $\vartheta = \vartheta(x) \in V_{1D}$ and for any $k = 1, \ldots, m$. The frequency coefficients $\widetilde{u}_j \in V_{1D}$ are the actual unknowns of the numerical problem. Solution to (3.6) requires to solve a system of coupled 1D problems. If the index m is small enough (e.g., $m \leq 10$), this procedure is expected to be more convenient than solving the complete problem (2.1). In practical applications, the appropriate choice of the index m represents a non-trivial task. Some examples will be provided in sections 3.4 and 4.3.

REMARK 1. *The conformity hypothesis i) can hold only if suitable assumptions are made on the boundary conditions and on the smoothness of the maps ψ_x. Non-homogeneous Dirichlet boundary conditions can be easily dealt with if, for instance, the Dirichlet data are given by linear combinations of the modal basis functions, i.e., in the form $\sum_{j\in J} c_j\varphi_j$, with $J \subset [1, m]$, mapped onto Γ_0 or Γ_1 (see, e.g., section 3.4.3). In this case, for all $1 \leq j \leq m$, non-homogeneous Dirichlet data equal to c_j if $j \in J$ and equal to zero otherwise are enforced on the frequency coefficients $\widetilde{v}_j$ at x_0 or x_1. In general we can impose any non homogeneous Dirichlet data after approximating it via the corresponding projection onto span$\{\varphi_k\}_{k=1}^m$.*

REMARK 2. *The rate of modal convergence depends on the adopted modal basis as well as on the regularity of u (see, e.g., [5, 8, 6, 7]). In the context of problems posed on thin domains, specific choices for the modal functions are discussed in [21, 22] to guarantee both asymptotically (as the plate thickness becomes infinitesimal) and spectrally (as the number of modes grows to infinity) optimal estimates of the modeling error.*

3.2. The case of 2D advection-diffusion-reaction problems. We particularize the reduced formulation (3.6) to a linear advection-diffusion-reaction (ADR) problem completed with full homogeneous Dirichlet boundary conditions. For the sake of simplicity we consider the 2D case. The full space V coincides with $H_0^1(\Omega)$, while V_{1D} coincides with $H_0^1(\Omega_{1D})$. Moreover, the modal functions φ_k vanish on Γ_*. The bilinear and linear forms in (2.1) are given by

$$a(u,v) = \int_\Omega \mu\nabla u\cdot\nabla v\,dxdy + \int_\Omega \left(\boldsymbol{\beta}\cdot\nabla u + \sigma u\right) v\,dxdy \quad \text{and} \quad \mathcal{F}(v) = \int_\Omega f v\,dxdy, \tag{3.7}$$

respectively, where $\boldsymbol{\beta} = (\beta_1, \beta_2)^T$. Usual regularity assumptions are made on the data to guarantee the well-posedness of such a weak formulation, namely $\mu \in L^\infty(\Omega)$, $\boldsymbol{\beta} \in [W^{1,\infty}(\Omega)]^2$, $\sigma \in L^\infty(\Omega)$, $f \in L^2(\Omega)$, μ is uniformly positive on Ω, and $\sigma - \frac{1}{2}\nabla\cdot\boldsymbol{\beta}$ is non-negative on Ω. Under these assumptions, the bilinear form $a(\cdot,\cdot)$ is $H_0^1(\Omega)$-coercive.

We exploit the gradient expansion

$$\nabla_{\mathbf{z}}\big(w(x)\,\varphi_s(\psi_x(y))\big) = \varphi_s(\psi_x(y)) \begin{bmatrix} \frac{dw(x)}{dx} \\ 0 \end{bmatrix} + w(x)\,\varphi_s'(\psi_x(y)) \begin{bmatrix} \mathcal{D}_1(\mathbf{z}) \\ \mathcal{D}_2(\mathbf{z}) \end{bmatrix} \tag{3.8}$$

for $s = 1, \dots, m$ and for any $w \in V_{1D}$, where $\nabla_{\mathbf{z}}$ is the gradient with respect to $\mathbf{z}$, while $\varphi_s'(\psi_x(y))$ stands for $d\varphi_s/d\widehat{y}$ at the point $\psi_x(y)$. Notice that $\mathcal{D}_2(\mathbf{z}) \equiv \partial\psi_x/\partial y$ is a scalar quantity since we are solving a 2D problem. The determinant $\big|\det\big(\mathcal{D}_2^{-1}\big(x, \psi_x^{-1}(\widehat{\mathbf{y}})\big)\big)\big|$ in (2.5) thus reduces to the absolute value $\big|\mathcal{D}_2^{-1}\big(x, \psi_x^{-1}(\widehat{y})\big)\big|$.

By applying (3.8) to each gradient of the bilinear form in (3.7) and by suitably reordering the resulting terms, we obtain the following system of 1D problems (we refer to [9] for the detailed computations): for $j, k = 1, \dots, m$, find $\widetilde{u}_j \in H_0^1(\Omega_{1D})$ such that, $\forall \vartheta \in H_0^1(\Omega_{1D})$,

$$\begin{aligned}
&\sum_{j=1}^{m} \Bigg\{ \int_{\Omega_{1D}} \Big[\widehat{r}_{kj}^{1,1}(x)\, \frac{d\widetilde{u}_j(x)}{dx}\, \frac{d\vartheta(x)}{dx} + \widehat{r}_{kj}^{1,0}(x)\, \frac{d\widetilde{u}_j(x)}{dx}\, \vartheta(x) + \widehat{r}_{kj}^{0,1}(x)\, \widetilde{u}_j(x)\, \frac{d\vartheta(x)}{dx} \\
&\quad + \widehat{r}_{kj}^{0,0}(x)\, \widetilde{u}_j(x)\, \vartheta(x) \Big]\, dx \Bigg\} = \int_{\Omega_{1D}} \Bigg[\int_{\widehat{\gamma}_1} f(x, \psi_x^{-1}(\widehat{y}))\varphi_k(\widehat{y})\, \big|\mathcal{D}_2^{-1}\big(x, \psi_x^{-1}(\widehat{y})\big)\big|\, d\widehat{y} \Bigg]\, \vartheta(x)\, dx,
\end{aligned} \tag{3.9}$$

with

$$\widehat{r}_{kj}^{s,t}(x) = \int_{\widehat{\gamma}_1} r_{kj}^{s,t}(x, \widehat{y})\, \big|\mathcal{D}_2^{-1}\big(x, \psi_x^{-1}(\widehat{y})\big)\big|\, d\widehat{y} \quad \text{for } s, t = 0, 1, \tag{3.10}$$

where

$$\begin{aligned}
r_{kj}^{1,1}(x,\widehat{y}) &= \mu\big(x, \psi_x^{-1}(\widehat{y})\big)\, \varphi_j(\widehat{y})\, \varphi_k(\widehat{y}), \\
r_{kj}^{0,1}(x,\widehat{y}) &= \mu\big(x, \psi_x^{-1}(\widehat{y})\big)\, \varphi_j'(\widehat{y})\, \varphi_k(\widehat{y})\, \mathcal{D}_1\big(x, \psi_x^{-1}(\widehat{y})\big), \\
r_{kj}^{1,0}(x,\widehat{y}) &= \mu\big(x, \psi_x^{-1}(\widehat{y})\big)\, \varphi_j(\widehat{y})\, \varphi_k'(\widehat{y})\, \mathcal{D}_1\big(x, \psi_x^{-1}(\widehat{y})\big) + \beta_1\big(x, \psi_x^{-1}(\widehat{y})\big)\, \varphi_j(\widehat{y})\, \varphi_k(\widehat{y}), \\
r_{kj}^{0,0}(x,\widehat{y}) &= \mu\big(x, \psi_x^{-1}(\widehat{y})\big)\, \varphi_j'(\widehat{y})\, \varphi_k'(\widehat{y}) \Big\{ \big[\mathcal{D}_1\big(x, \psi_x^{-1}(\widehat{y})\big)\big]^2 + \big[\mathcal{D}_2\big(x, \psi_x^{-1}(\widehat{y})\big)\big]^2 \Big\} \\
&\quad + \varphi_j'(\widehat{y})\, \varphi_k(\widehat{y}) \Big\{ \beta_1\big(x, \psi_x^{-1}(\widehat{y})\big)\, \mathcal{D}_1\big(x, \psi_x^{-1}(\widehat{y})\big) + \beta_2\big(x, \psi_x^{-1}(\widehat{y})\big)\, \mathcal{D}_2\big(x, \psi_x^{-1}(\widehat{y})\big) \Big\} \\
&\quad + \sigma\big(x, \psi_x^{-1}(\widehat{y})\big) \varphi_j(\widehat{y})\, \varphi_k(\widehat{y}).
\end{aligned}$$

The quantities $\widehat{r}_{kj}^{s,t}$ collect the transverse contributions. We also observe that using the map ψ_x, the reduced system is fully solved on the reference rectangle $\widehat{\Omega}$ in place of the physical domain Ω.

Let $\mathfrak{u} = (\widetilde{u}_1, \dots, \widetilde{u}_m)$ and $\mathfrak{v} = (\vartheta_1, \dots, \vartheta_m)$ be in $W = [H_0^1(\Omega_{1D})]^m$. Let $\mathfrak{D}$, $\mathfrak{A}$, $\mathfrak{B}$, and $\mathfrak{R}$ be $\mathbb{R}^{m,m}$-valued fields defined on Ω_{1D} such that, for $j, k = 1, \dots, m$ and

$x \in \Omega_{1D}$,

$$\mathfrak{D}_{kj}(x) = \widehat{r}_{kj}^{1,1}(x),$$
$$\mathfrak{A}_{kj}(x) = \widehat{r}_{jk}^{0,1}(x),$$
$$\mathfrak{B}_{kj}(x) = \int_{\widehat{\gamma}_1} \beta_1\big(x, \psi_x^{-1}(\widehat{y})\big)\, \varphi_j(\widehat{y})\, \varphi_k(\widehat{y})\, \big|\mathcal{D}_2^{-1}\big(x, \psi_x^{-1}(\widehat{y})\big)\big|\, d\widehat{y},$$
$$\mathfrak{R}_{kj}(x) = \widehat{r}_{kj}^{0,0}(x).$$

Then, the left-hand side of the reduced problem (3.9) defines the bilinear form

$$\mathfrak{a}(\mathfrak{u}, \mathfrak{v}) = \int_{\Omega_{1D}} \left[\mathfrak{D} \frac{d\mathfrak{u}}{dx} \cdot \frac{d\mathfrak{v}}{dx} + (\mathfrak{A} + \mathfrak{B}) \frac{d\mathfrak{u}}{dx} \cdot \mathfrak{v} + \mathfrak{A}^T \mathfrak{u} \cdot \frac{d\mathfrak{v}}{dx} + \mathfrak{R}\mathfrak{u} \cdot \mathfrak{v} \right] dx. \tag{3.11}$$

Integrating by parts the third term on the right-hand side and assuming enough smoothness to define $\frac{d}{dx}\mathfrak{A}$ leads to

$$\mathfrak{a}(\mathfrak{u}, \mathfrak{v}) = \int_{\Omega_{1D}} \left[\mathfrak{D} \frac{d\mathfrak{u}}{dx} \cdot \frac{d\mathfrak{v}}{dx} + (\mathfrak{A} - \mathfrak{A}^T) \frac{d\mathfrak{u}}{dx} \cdot \mathfrak{v} + \mathfrak{B} \frac{d\mathfrak{u}}{dx} \cdot \mathfrak{v} + \Big(\mathfrak{R} - \frac{d\mathfrak{A}^T}{dx} \Big) \mathfrak{u} \cdot \mathfrak{v} \right] dx. \tag{3.12}$$

The first term on the right-hand side corresponds to a diffusion contribution since the matrix $\mathfrak{D}$ is symmetric and uniformly positive definite; the third term represents an advection contribution since the matrix $\mathfrak{B}$ is symmetric; the last term corresponds to a reaction term. We observe that the second term cannot be directly identified with an advection term since the matrix $(\mathfrak{A} - \mathfrak{A}^T)$ is skew-symmetric. We emphasize that the properties of the bilinear form $\mathfrak{a}(\cdot,\cdot)$ on W are inherited directly from those of the bilinear form $a(\cdot,\cdot)$ associated with the full problem. In particular, equipping W with the norm $\|\mathfrak{u}\|_W = \|E\mathfrak{u}\|_{H^1(\Omega)}$, with the extension operator

$$E : W \ni \mathfrak{u} \longmapsto E\mathfrak{u}(x,y) = \sum_{k=1}^{m} \widetilde{u}_k(x) \varphi_k(\psi_x(y)) \in H_0^1(\Omega), \tag{3.13}$$

the above assumptions imply that $\mathfrak{a}(\cdot,\cdot)$ is W-coercive.

REMARK 3. *Computations in (3.9) simplify under particular assumptions on the data. For instance, for constant coefficients μ, $\boldsymbol{\beta}$, and σ, the orthonormality condition (3.1) implies that $\widehat{r}_{kj}^{1,1} = 0$ if $k \neq j$, as well as all the terms multiplied by $\varphi_j(\widehat{y})\, \varphi_k(\widehat{y})$ provide a non-zero contribution only for $k = j$. A further interesting simplification occurs when the map ψ_x is affine, since $\mathcal{D}_2\big(\mathbf{z}\big)$ reduces to $L(x)^{-1}$. In particular, when the physical domain itself coincides with a rectangle (i.e., L=constant in (2.3)), all the terms involving $\mathcal{D}_1\big(\mathbf{z}\big)$ vanish.*

REMARK 4. *As peculiar simplification, we consider the 2D Poisson equation ((3.7) with $\mu = 1$, $\boldsymbol{\beta} = \mathbf{0}$, $\sigma = 0$) completed with full homogeneous Dirichlet boundary conditions. We make the simplest possible choice for the reduced space V_m by setting $m = 1$ in (3.2). Then we resort to the linear map (2.3), assuming $L \in C^2(\Omega_{1D})$. The coefficients in (3.10) simplify into*

$$\widehat{r}_{11}^{1,1}(x) = L(x), \quad \widehat{r}_{11}^{1,0}(x) = \widehat{r}_{11}^{0,1}(x) = \frac{L'(x)}{2},$$
$$\widehat{r}_{11}^{0,0}(x) = \frac{1}{L(x)} \int_{\widehat{\gamma}_1} \big[\varphi_1'(\widehat{y})\big]^2 \Big\{ \big[L'(x)\, \widehat{y}\big]^2 + 1 \Big\}\, d\widehat{y}.$$

The reduced formulation (3.9) thus becomes: find $\widetilde{u}_1 \in H^1_0(\Omega_{1D})$ *such that*

$$\int_{\Omega_{1D}} L(x)\,\frac{d\widetilde{u}_1(x)}{dx}\,\frac{d\vartheta(x)}{dx}\,dx + \int_{\Omega_{1D}} L(x)\,\gamma(x)\,\widetilde{u}_1(x)\,\vartheta(x)\,dx = \int_{\Omega_{1D}} L(x)\,\widetilde{f}_1(x)\,\vartheta(x)\,dx,$$

where

$$\gamma(x) = \frac{1}{\big[L(x)\big]^2}\int_{\widehat{\gamma}_1}\big[\varphi_1'(\widehat{y})\big]^2\Big\{\big[L'(x)\,\widehat{y}\big]^2+1\Big\}\,d\widehat{y} - \frac{L''(x)}{2L(x)}$$

is the reactive coefficient of the reduced formulation, and $\widetilde{f}_1$ *is the (first) frequency coefficient associated with the forcing term* f*, according to definition (3.3). The coefficient* γ *further simplifies into* $\big[L(x)\big]^{-2}\int_{\widehat{\gamma}_1}\big[\varphi_1'(\widehat{y})\big]^2\,d\widehat{y}$ *when* Ω *itself coincides with a rectangle (since* $L'(x) = L''(x) = 0$*).*

REMARK 5. *We highlight that even a purely diffusive problem (i.e.,* $\boldsymbol{\beta} = \mathbf{0}$ *and* $\sigma = 0$ *in (3.7)) yields low-order contributions in the reduced framework. However, the first-order terms yielded by the hierarchical reduction are always weighted by the diffusive coefficient* μ *itself. Consequently possible instabilities due to a dominant advection or reaction should be in general avoided provided that the deformation indices* $\mathcal{D}_1(\mathbf{z})$ *and* $\mathcal{D}_2(\mathbf{z})$ *are small enough.*

3.3. Discretization of the reduced problem. Since the reduced formulation actually coincides with a system of equations posed on the 1D domain, we have to introduce a partition of Ω_{1D} to obtain the discrete counterpart of (3.4). Let $\mathcal{T}_h$ be a subdivision of Ω_{1D} into subintervals $K_j = (x_{j-1}, x_j)$ of width $h_j = x_j - x_{j-1}$, and set $h = \max_j h_j$. We introduce a conforming finite element space $V^h_{1D} \subset V_{1D}$ associated with the partition $\mathcal{T}_h$, such that $\dim(V^h_{1D}) = N_h < +\infty$. Then we add the following assumption:

iii) *density* hypothesis:

$$\forall u_{1D} \in V_{1D} \qquad \lim_{h\to 0} d_{1D}(u_{1D}, V^h_{1D}) = 0,$$

where $d_{1D}(\cdot,\cdot)$ denotes the distance induced by the norm $\|\cdot\|_{V_{1D}} := \|\cdot\|_{H^1(\Omega_{1D})}$ in V_{1D}.

The *discrete reduced formulation* can thus be stated as

$$\text{find } u^h_m \in V^h_m \quad : \quad a(u^h_m, v^h_m) = \mathcal{F}(v^h_m) \quad \forall v^h_m \in V^h_m, \tag{3.14}$$

where the space V^h_m is given by

$$V^h_m = \Big\{ v^h_m(x,\mathbf{y}) = \sum_{k=1}^{m} \widetilde{v}^h_k(x)\,\varphi_k(\psi_x(\mathbf{y})),\ \text{with } \widetilde{v}^h_k \in V^h_{1D},\ x \in \Omega_{1D},\ \mathbf{y} \in \gamma_x \Big\}. \tag{3.15}$$

Because of the conformity assumption on the discrete space V^h_{1D}, there holds

$$V^h_m \subset V_m. \tag{3.16}$$

3.3.1. Convergence. We denote with $e_m^h = u - u_m^h \in V$ the *global error* taking into account both the model $(u - u_m)$ and the discretization $(u_m - u_m^h)$ error contribution. The following convergence result holds.

PROPOSITION 3.1. *Let u be the solution to the full problem (2.1) and let u_m^h solve the reduced discrete problem (3.14). There holds*

$$\lim_{m\to+\infty} \lim_{h\to 0} u_m^h = u \quad \text{in } V.$$

Proof. Fix $m \geq 1$. Using the conformity relation $V_m^h \subset V_m$, it is readily inferred that

$$\|u_m - u_m^h\|_V \leq C \inf_{v_m^h \in V_m^h} \|u_m - v_m^h\|_V,$$

with C a constant depending on the continuity and coercivity constants of the bilinear form $a(\cdot,\cdot)$. Moreover, for all $v_m^h \in V_m^h$,

$$(u_m - v_m^h)(x,\mathbf{y}) = \sum_{k=1}^{m} \left[\widetilde{u}_k(x) - \widetilde{v}_k^h(x)\right] \varphi_k(\psi_x(\mathbf{y})),$$

with $\widetilde{u}_k \in V_{1D}$ and $\widetilde{v}_k^h \in V_{1D}^h$, for all $k = 1,\dots,m$. It is clear that there exists a constant C', depending on ψ_x, for every $x \in \Omega_{1D}$, and on the set $\{\varphi_k\}_{k=1}^m$, such that

$$\|u_m - v_m^h\|_V \leq C' \sum_{k=1}^{m} \|\widetilde{u}_k - \widetilde{v}_k^h\|_{V_{1D}}.$$

Since m is fixed, the density assumption *iii*) guarantees that this upper bound tends to zero as $h \to 0$. Hence,

$$\lim_{h\to 0} u_m^h = u_m \quad \text{in } V.$$

Letting $m \to +\infty$ yields the conclusion. □

Concerning the rate of convergence of the whole reduction procedure (model reduction plus finite element discretization) some results are already available in the literature. In [6] a combined Fourier–finite element method is used to approximate an elliptic problem and error estimates, additively depending on h and m, are derived with respect to anisotropic Sobolev norms. The same kind of analysis is pursued in [7] where a 3D Navier-Stokes problem with one direction of periodicity is approximated via a Fourier pseudo-spectral scheme along such a direction and by means of finite elements with respect to the other directions. A Fourier-finite element approach is applied in [13] to the 3D Poisson equation solved on an axisymmetric domain with reentrant edges. L^2– and H^1–convergence results, preserving the splitting between the modal index and the discretization step contributions, are derived. We refer to section 3.4.1 for a numerical convergence study of the discrete reduced formulation (3.14).

3.3.2. Algebraic formulation. The discrete counterpart of the 1D system (3.6) is the following: find $\{\widetilde{u}_j^h\}_{j=1}^m \in [V_{1D}^h]^m$, such that

$$\sum_{j=1}^{m} a(\widetilde{u}_j^h \varphi_j, \vartheta_l \varphi_k) = \mathcal{F}(\vartheta_l \varphi_k) \tag{3.17}$$

with $k = 1, \ldots, m$, and where ϑ_l, for $l = 1, \ldots, N_h$, is a generic basis function of the discrete space V_{1D}^h. By expanding the unknown coefficients $\widetilde{u}_j^h$ in terms of the finite element basis $\{\vartheta_i\}_{i=1}^{N_h}$ (i.e., $\widetilde{u}_j^h(x) = \sum_{i=1}^{N_h} \widetilde{u}_{j,i}^h \vartheta_i(x)$) and by suitably varying the indices k and l, we obtain a linear system characterized by a $mN_h \times mN_h$ block matrix A, whose pattern is represented in Figure 3.1. The indices k and j, associated with the modes, identify the "macro-structure" of A, i.e., run on the block-rows and block-columns, respectively; on the other hand, the indices l and i, related to the finite element basis, span the rows and columns, respectively of each block. Each

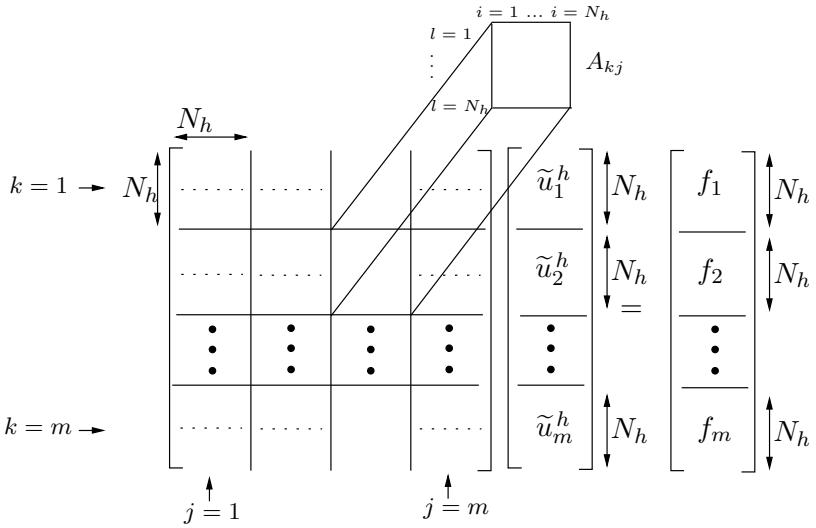

FIG. 3.1. *Sketch of the linear system corresponding to the discrete reduced formulation (3.17), with* $[f_k]_l = \mathcal{F}(\vartheta_l \varphi_k)$*, for* $k = 1, \ldots, m$ *and* $l = 1, \ldots, N_h$*.*

$N_h \times N_h$-block A_{kj} preserves the sparsity pattern peculiar to the adopted finite element approximation. This provides two advantages. First of all, a 1D finite element matrix can be characterized by a structured sparsity pattern, with benefits both in storing and solving the associated system. Moreover, all the coupled 1D problems in (3.17) share the same pattern, that can be consequently stored once for all.

3.4. Numerical tests. The reliability and effectiveness of the global model reduction is numerically investigated in a 2D framework. For this purpose the choice of the reduced space V_m is clearly a crucial issue. A priori it should stem from a trade-off between the need to capture the main features of the full solution and the necessity to limit the computational costs. In the numerical experiments we adopt the most straightforward approach (a sort of trial-and error strategy): we compute the approximate solution u_m^h starting from $m = 1$; then we gradually increase such a value until a sort of "stagnation" (no significative change occurs from a qualitative viewpoint) is detected in the reduced solution. A more mathematically sound technique will be proposed in [16] in view of an automatic selection of m.

In section 3.4.1 we study the convergence of this procedure on two test cases with analytical solution. In the two subsequent sections, we assess the performance of the approach on two test cases where local transverse dynamics are induced either by a strong heterogeneity in a problem coefficient (section 3.4.2) or by the shape of the domain Ω (section 3.4.3). We use continuous piecewise linear finite elements to

generate the space V_{1D}^h, while we employ sinusoidal functions for the modal basis $\{\varphi_k\}_k$. In all cases, homogeneous Dirichlet boundary conditions are enforced on the boundary Γ_*. To compute the integrals of the sine functions we employ at least four quadrature nodes per wavelength (Gaussian quadrature formulas).

3.4.1. Test cases with analytical solutions. As a consequence of the selection of a sinusoidal-finite element discretization, convergence rates can be inferred from the results in [6], where a (complete) Fourier expansion is used along the transverse directions. Consider the anisotropic Sobolev space

$$H^{r,s}(\Omega_{1D} \times \widehat{\gamma}_1) = L^2(\widehat{\gamma}_1; H^r(\Omega_{1D})) \cap H^s(\widehat{\gamma}_1; L^2(\Omega_{1D})),$$

where $r, s \geq 0$ are integers, $L^2(\rho; X) = \big\{w : \rho \to X \text{ measurable s.t. } \int_\rho \|w(\eta)\|_X^2 \, d\eta < +\infty\big\}$, $H^s(\rho; Y) = \big\{w \in L^2(\rho; Y) \text{ s.t. } \partial^k w/\partial \eta^k \in L^2(\rho; Y) \text{ for } 0 \leq k \leq s\big\}$, with $\rho \subset \mathbb{R}$ and X and Y Hilbert spaces. Let $H_p^{r,s}(\Omega_{1D} \times \widehat{\gamma}_1)$ define the closure, with respect to the graph-norm on $H^{r,s}(\Omega_{1D} \times \widehat{\gamma}_1)$, of the space $C_p^\infty(\Omega_{1D} \times \widehat{\gamma}_1)$ of the C^∞-functions periodic, together with all their derivatives, with respect to the y-direction (see [12, 14] for more details).

Using sine functions in the modal expansion precludes a priori any spectral convergence rate, even with smooth solutions, e.g., C^∞-functions (see [5]). If the exact solution belongs to $H_p^{2,2}(\widehat{\Omega})$, the expected convergence result for e_m^h is the one stated in Theorems 2.1 and 3.2 in [6], namely quadratic for the L^2-norm and linear for the H^1-norm, with respect to both m^{-1} and h.

Test case 1. The analytical solution is chosen to be $u_1(x, y) = y^2\,(1-y)^2\,(0.75-y)\,x\,(2-x)$, with $(x, y) \in \widehat{\Omega} = (0, 2) \times (0, 1)$, so that $u_1 \in H_p^{2,2}(\widehat{\Omega})$. Figure 3.2 and Tables 3.1 and 3.2 collect the values of the error with respect to both the L^2- and the H^1-norm. The expected dependence of the error on m is evident for h small enough. For high values of m the convergence rate is biased by the discretization error. The L^2-norm is more strongly affected by the choice made for the discretization step. The choice $h = 0.05$ is the only exception, the order 2 being preserved, at least till $m = 32$. On the contrary, the H^1-norm exhibits a slight superconvergence, already for rather large values of h (the reduction factor of $\|e_m^h\|_{H^1(\widehat{\Omega})}$ is about 2.5, for a fixed h). Concerning the convergence of e_m^h with respect to the discretization step, we observe a marginal sensitivity to the mesh size, at least until a sufficiently high number of transverse modes is reached. This trend is particularly evident for the H^1-norm (all the curves coincide until $m = 8$ in Figure 3.2, right) and can be ascribed to the dominance of the modeling error over the discretization error.

TABLE 3.1
L^2–norm of the global error for test case 1.

m	$h = 0.4$	$h = 0.2$	$h = 0.1$	$h = 0.05$
1	6.4002e-03	6.3963e-03	6.3961e-03	6.3961e-03
2	1.8722e-03	1.8544e-03	1.8534e-03	1.8533e-03
4	6.2963e-04	5.7332e-04	5.6989e-04	5.6968e-04
8	3.0156e-04	1.5193e-04	1.3840e-04	1.3753e-04
16	2.6991e-04	7.0620e-05	3.2539e-05	2.8613e-05
32	2.6848e-04	6.4911e-05	1.6881e-05	6.6991e-06

TABLE 3.2
H^1–norm of the global error for test case 1.

m	$h = 0.4$	$h = 0.2$	$h = 0.1$	$h = 0.05$
1	4.5228e-02	4.5220e-02	4.5220e-02	4.5220e-02
2	2.1754e-02	2.1720e-02	2.1718e-02	2.1718e-02
4	1.1480e-02	1.1410e-02	1.1405e-02	1.1405e-02
8	5.1457e-03	4.9812e-03	4.9714e-03	4.9708e-03
16	2.3528e-03	1.9656e-03	1.9406e-03	1.9390e-03
32	1.5137e-03	7.8628e-04	7.2129e-04	7.1716e-04

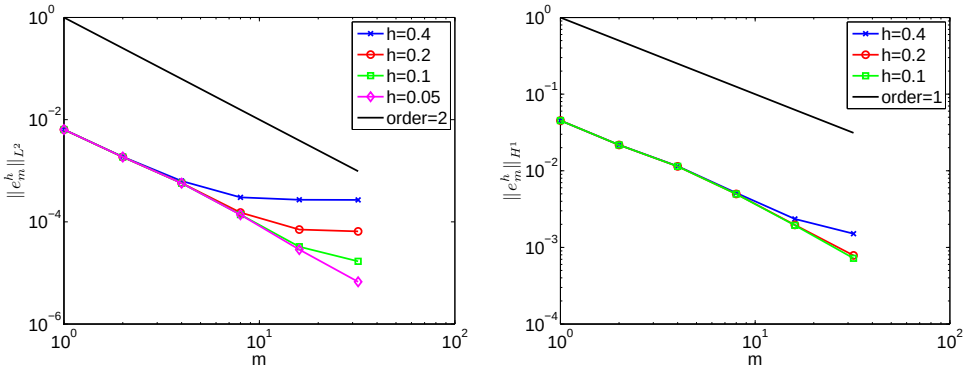

FIG. 3.2. *Test case 1: modal convergence of the global error for different choices of the step h: L^2–norm (left), H^1–norm (right).*

Test case 2. The analytical solution is now chosen to be $u_2 = y^2\,(1-y)^2\,(0.75-y)\,x\,(2-x)\,\exp(\sin(2\pi x))$ on $\widehat{\Omega} = (0,2)\times(0,1)$, so that $u_2 \in H_p^{2,2}(\widehat{\Omega})$. We summarize the corresponding results in Figure 3.3 and in Tables 3.3 and 3.4. Notice the different choice made for m and h with respect to Figure 3.2. The x-variations of the function u_2 require now a finer finite element discretization step with respect to function u_1. A different behavior of the H^1-error is observed in terms of modal convergence (compare with Figure 3.2, right). The expected linear modal convergence is now achieved only for h small enough, and the superconvergence is less marked with respect to the first test case. On the contrary, the discrepancy between u_1 and u_2 is less striking if we consider the L^2-norm of the error (compare with Figure 3.2, left), even if to achieve quadratic modal convergence, a smaller h is required for u_2. Concerning the finite element convergence, we observe for u_2 a greater sensitivity of the error to the value chosen for h. Moreover, fewer modes are now sufficient to detect the expected convergence rate, at least when the step h is large enough, so that the discretization error is not dominated by the modeling one.

TABLE 3.3
L^2–norm of the global error for test case 2.

m	$h = 0.2$	$h = 0.1$	$h = 0.05$	$h = 0.025$	$h = 0.0125$
1	9.7946e-03	9.6712e-03	9.6628e-03	9.6622e-03	9.6622e-03
2	3.3444e-03	2.8388e-03	2.8022e-03	2.7998e-03	2.7997e-03
4	2.0354e-03	9.8200e-04	8.6881e-04	8.6109e-04	8.6060e-04
8	1.8575e-03	5.1679e-04	2.3959e-04	2.0980e-04	2.0779e-04
16	1.8464e-03	4.7517e-04	1.2691e-04	5.2235e-05	4.3452e-05

TABLE 3.4
H^1–norm of the global error for test case 2.

m	$h = 0.2$	$h = 0.1$	$h = 0.05$	$h = 0.025$	$h = 0.0125$
1	8.3525e-02	7.8041e-02	7.7221e-02	7.7153e-02	7.7149e-02
2	5.0836e-02	3.7018e-02	3.4631e-02	3.4428e-02	3.4415e-02
4	4.1715e-02	2.2288e-02	1.7952e-02	1.7552e-02	1.7524e-02
8	3.8655e-02	1.5718e-02	8.5003e-03	7.6166e-03	7.5533e-03
16	3.8031e-02	1.4096e-02	4.8870e-03	3.1033e-03	2.9445e-03

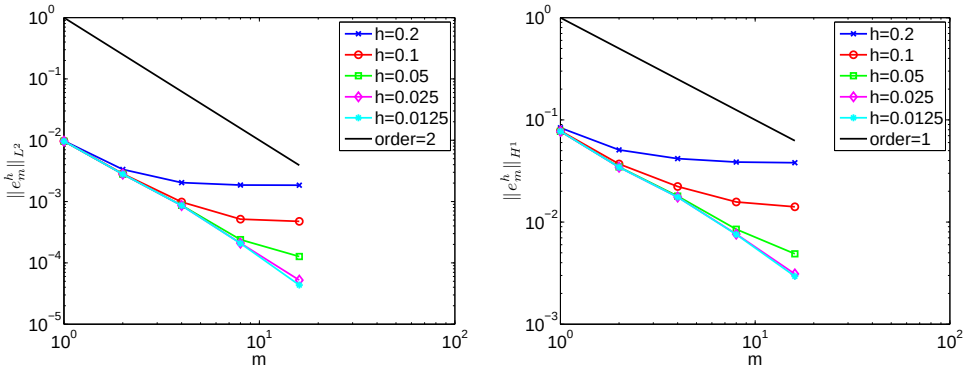

FIG. 3.3. *Test case 2: modal convergence of the global error for different choices of the step h: L^2–norm (left), H^1–norm (right).*

3.4.2. Test case 3: diffusion heterogeneity. For the sake of simplicity we assume henceforth the partition $\mathcal{T}_h$ to be sufficiently fine to neglect the discretization error. The physical domain Ω coincides with the trapezoidal portion of $\mathbb{R}^2$ bounded, counterclockwise, by the straight lines $x = 0$, for $0 \le y \le 1$; $y = -0.1x$, for $0 \le x \le 4$; $x = 4$, for $-0.4 \le y \le 1.4$; $y = 1 + 0.1x$, for $0 \le x \le 4$. We solve the pure diffusive problem $-\nabla \cdot (\mu \nabla u) = f$, completed with full homogeneous Dirichlet boundary conditions. The viscous coefficient is $\mu(x, y) = 1 + 100\,\chi_D(x, y)$ so that it takes on large values in the circular region $D = \{(x, y) : (x-1)^2 + (y-0.25)^2 < 0.1\}$ only, with χ_D the characteristic function associated with D. The source term is selected identically equal to 1. Figure 3.4, top-left, shows the corresponding (full) solution u. The area where the viscosity is larger can be easily recognized by the deformation of the contour lines.

We apply the global model reduction procedure moving from the computationally cheapest choice $m = 1$ up to $m = 9$. Figure 3.4 gathers the contour plots of the discrete reduced solutions corresponding to the values $m = 1, 3, 5, 7, 9$, and for $h = 0.05$. It is evident that the accuracy of u_m^h increases as m gets larger. The local variation of the diffusion coefficient requires a rather large number of modes overall. While a few modal functions (e.g., 3) are enough to capture the behavior of u in the region $1.7 \le x \le 4$, at least 7 modes are necessary to get a sufficiently detailed approximation to the full solution, matching the behavior of u also in correspondence with D. No relevant change occurs when moving from $m = 7$ to $m = 9$.

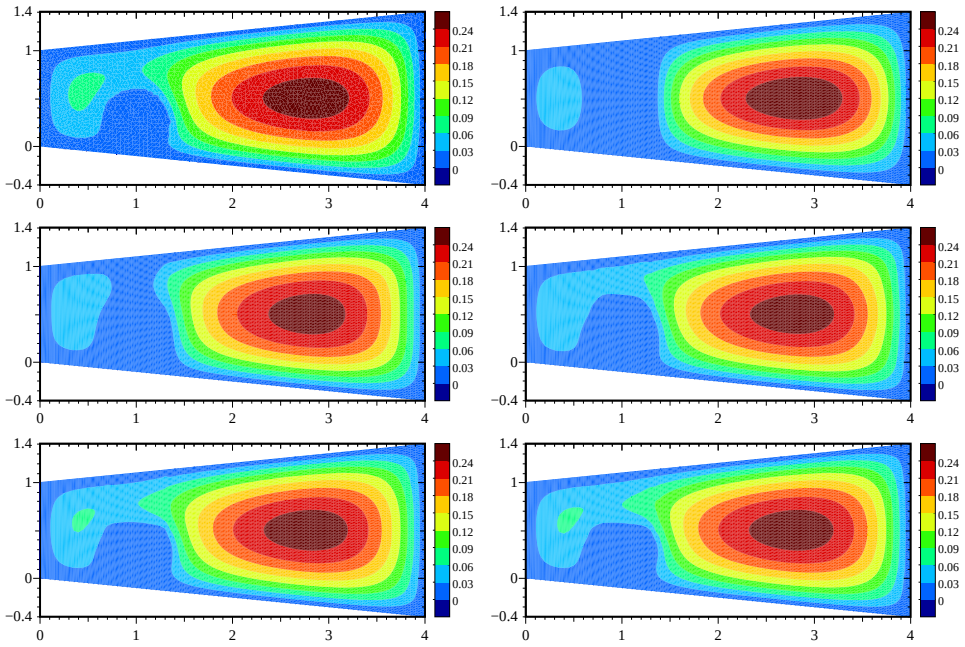

FIG. 3.4. *Global model reduction (test case 3): full solution and reduced approximations* u_1^h, u_3^h, u_5^h, u_7^h, u_9^h *(top-bottom, left-right).*

3.4.3. Test case 4: the wavy channel. This test case is of interest in haemodynamics, modeling a Bellhouse oxygenator for extra-corporeal circulation (see, e.g, [4]). In particular, we model oxygen transport inside a wavy channel consisting of two symmetric sinusoidal sections (see Figure 3.5). This geometry is typical of mass transfer devices such as blood oxygenators or membrane separators.

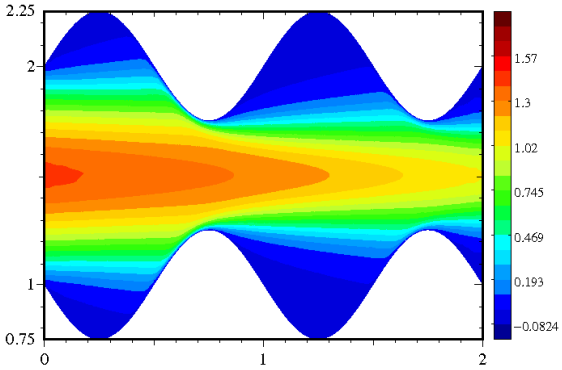

FIG. 3.5. *Wavy channel test case : full solution.*

The computational domain coincides with the region of $\mathbb{R}^2$ whose boundaries are defined by the functions (listed in counterclockwise order) $x = 0$, for $1 \leq y \leq 2$; $y = 1 - 0.25\sin(2\pi x)$, for $0 \leq x \leq 2$; $x = 2$, for $1 \leq y \leq 2$; $y = 2 + 0.25\sin(2\pi x)$, for $0 \leq x \leq 2$. We solve here the advection-diffusion problem (3.7) with $\sigma = 0$, $\mu(x, y) = 1$, and $\boldsymbol{\beta}(x, y) = (100, 0)^T$. The solution u represents the oxygen concentration in the

blood. The problem is completed with mixed boundary conditions. In particular we assign a nonhomogeneous Dirichlet condition at the inflow, by prescribing $u(x,y) = \sqrt{2}\,\sin(2\pi y)$ at the inflow $x = 0$; a homogeneous Dirichlet condition on the curved boundaries; a homogeneous Neumann condition at the outflow $x = 2$. Finally we choose as forcing term $f \equiv 0$.
The corresponding (full) solution u is displayed in Figure 3.5. Notice how the main stream of the motion, driven by the field $\boldsymbol{\beta}$, is modified by the irregular shape of the domain. This triggers transverse dynamics as shown by the bending of the contour lines.

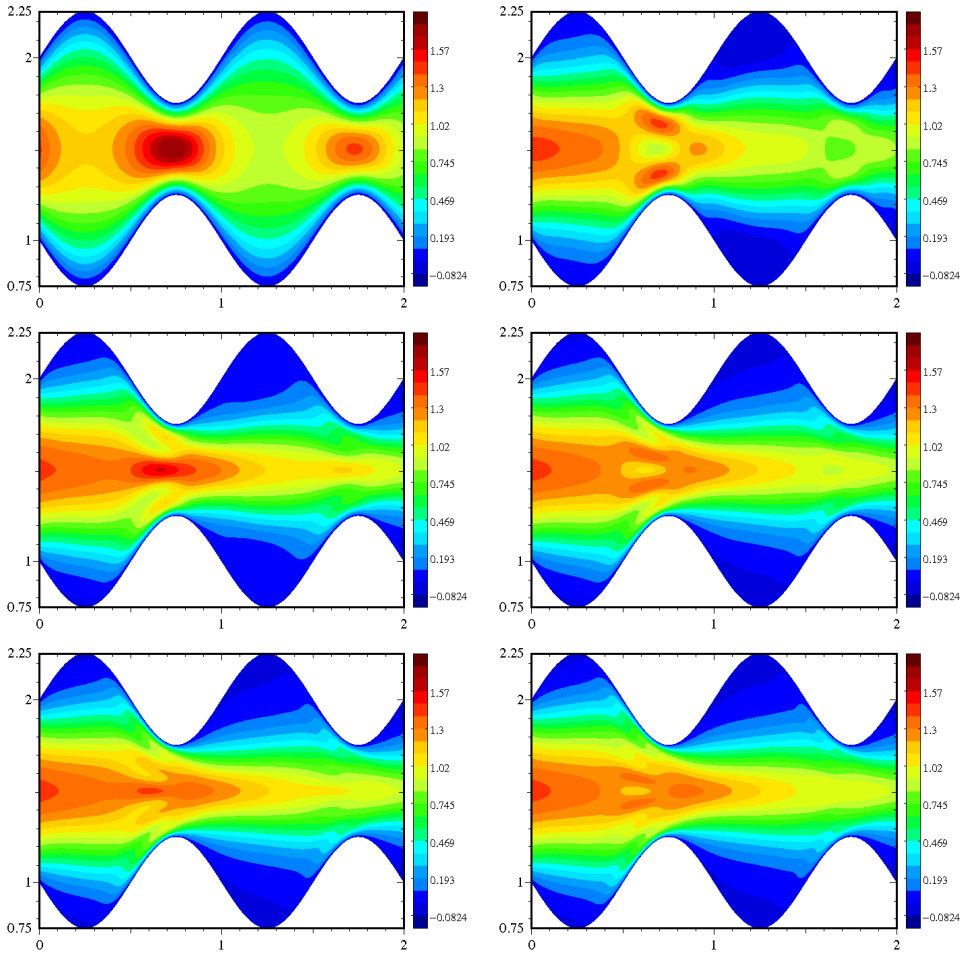

FIG. 3.6. *Global model reduction (wavy channel test case). reduced approximations* u_1^h, u_3^h, u_5^h, u_7^h, u_9^h, u_{11}^h *(top-bottom, left-right).*

We resort to the global model reduction procedure to approximate u, starting from $m = 1$ and then choosing larger values. In Figure 3.6 we show the contour plots of the discrete reduced solutions u_1^h, u_3^h, u_5^h, u_7^h, u_9^h, and u_{11}^h, for $h = 0.01$. We do not resort to any stabilization scheme since the choice made for h guarantees that the local Péclet number corresponding to an advective field $(100, 0)^T$ is strictly less than 1. However, the actual advective term in the reduced formulation (3.9) depends also

on $\mathcal{D}_1(\mathbf{z})$. This last contribution could make locally the chosen h insufficient to ensure the stability of the discretization scheme. This could explain the negative minimum values associated with some of the reduced solutions (-0.0824 for u_3^h, -0.0069 for u_7^h), in contrast to the minimum value 0 of the full solution (to make a fair comparison between the full and reduced frameworks, we have employed the same color map in all the contour-plots, ranging from the minimum to the maximum value of the reduced solutions). In contrast to test case 3, the full solution exhibits a complex behavior on the whole domain. Thus small values of m do not ensure enough accuracy to the reduced solution: at least $m = 9$ modes have to be employed to achieve a reasonable approximation.

4. Local model reduction. The strategy proposed in the previous section to select the reduced space exhibits an evident drawback: to accurately approximate a full solution with *local* strong transverse components, we are compelled to use a large number of modes over the whole domain, i.e., also where the transverse dynamics are not relevant. For instance, in the example of Figure 3.4, three sine functions guarantee a reliable reduced solution on the right half of the domain, while at least nine modes have to be employed in the left half. This implies an unnecessary increase of the computational costs. A computationally more effective approach consists in employing different values for m in different parts of the domain. Large values for m are associated with the zones where the transverse dynamics are meaningful, while small values are selected where the 1D behavior is dominant. We refer to this last approach as *local model reduction* in contrast to the global model reduction addressed in section 3.

4.1. Formulation of the locally reduced problem. The key point in local model reduction is to couple reduced solutions with a different number of modal components on various subdomains of Ω. In principle, the modal index can change in correspondence with each element K_j of the partition $\mathcal{T}_h$. In practice, a few subdomains of Ω_{1D}, grouping consecutive elements, are used, each featuring a fixed value of m. For this reason, we introduce a partition of Ω_{1D} into s non-overlapping macro subintervals $\Omega_{1D,i}$, with $i = 1, \dots, s$, such that $\cup_{i=1}^{s} \overline{\Omega}_{1D,i} = \overline{\Omega}_{1D}$, and the corresponding multi-index $\mathbf{m} = \{m_i\}_{i=1}^{s}$ collecting the number of modes selected on each $\Omega_{1D,i}$. We consequently identify in Ω the subdomains $\Omega_i = \bigcup_{x \in \Omega_{1D,i}} \{x\} \times \gamma_x$, for $i = 1, \dots, s$.

To formulate the locally reduced problem and its finite element discretization in the case of a modal multi-index $\mathbf{m}$, we need to modify the definition of the reduced spaces in (3.2) and (3.15). Accordingly, we first introduce the space

$$V_{\mathbf{m}} = \Big\{ v_{\mathbf{m}}(x,\mathbf{y}) : v_{\mathbf{m}}(x,\mathbf{y})\big|_{\Omega_{1D,i}} = \sum_{k=1}^{m_i} \widetilde{v}_k\big|_{\Omega_{1D,i}}(x)\, \varphi_k(\psi_x(\mathbf{y})) \\ \forall i = 1, \dots, s, \text{ with } \widetilde{v}_k \in V_{1D},\, x \in \Omega_{1D},\, \mathbf{y} \in \gamma_x \Big\},$$

resorting to m_i modal functions on each $\Omega_{1D,i}$ for $i = 1, \dots, s$. When we move from $\Omega_{1D,\,j}$ to $\Omega_{1D,\,j+1}$, for $j = 1, \dots, s-1$, we are a priori in the presence of a *model discontinuity* if $m_j \neq m_{j+1}$ (see Remark 6 for the details). As a result, $V_{\mathbf{m}}$ is not necessarily a subspace of V and we set $V'_{\mathbf{m}} = V_{\mathbf{m}} \cap V$.

Likewise the multi-index discrete reduced space is defined as

$$V^h_{\mathbf{m}} = \Big\{ v^h_{\mathbf{m}}(x,\mathbf{y}) : v^h_{\mathbf{m}}(x,\mathbf{y})\big|_{\Omega_{1D,i}} = \sum_{k=1}^{m_i} \widetilde{v}^h_k\big|_{\Omega_{1D,i}}(x)\,\varphi_k(\psi_x(\mathbf{y})) \\ \forall\, i = 1,\dots,s, \text{ with } \widetilde{v}^h_k \in V^h_{1D},\, x \in \Omega_{1D},\, \mathbf{y} \in \gamma_x \Big\}.$$

Again, because of possible model discontinuities, $V^h_{\mathbf{m}}$ is not necessarily a conforming approximation space of V and we set $V^{h\,\prime}_{\mathbf{m}} = V^h_{\mathbf{m}} \cap V$.

The local reduced formulation and the corresponding finite element discretization take the form (3.4) and (3.14), the spaces V_m and V^h_m being replaced by $V'_{\mathbf{m}}$ and $V^{h\,\prime}_{\mathbf{m}}$, respectively. To enforce the matching at model discontinuities so as to work directly with the spaces $V_{\mathbf{m}}$ and $V^h_{\mathbf{m}}$, we consider a domain decomposition approach (see Remark 6). This is the focus of the next section.

4.2. A domain decomposition approach. Subdomains with a different number of modal functions are connected via an *iterative substructuring method*. This approach is new in this context. Alternative techniques based on an appropriate redefinition of the reduced space are pursued, e.g., in [1, 3, 23].

For the sake of simplicity we consider the case of two macro subintervals $\Omega_{1D,1}$ and $\Omega_{1D,2}$, separated by $\xi \in \Omega_{1D}$. Let $\{\xi\} \times \gamma_\xi$ be the interface between $\Omega_1 = \bigcup_{x\in\Omega_{1D,1}} \{x\} \times \gamma_x$ and $\Omega_2 = \bigcup_{x\in\Omega_{1D,2}} \{x\} \times \gamma_x$. The modal index m is set to m_1 and m_2 on Ω_1 and Ω_2, respectively. We denote with $u^h_{m_i}$, for $i = 1, 2$, the restriction to Ω_i of the discrete reduced solution $u^h_{\mathbf{m}}$. Finally we assume homogeneous Dirichlet boundary conditions on Γ_0 and Γ_1.

Let us define the spaces $V^h_{m_i}$ and $V^h_{m_i,0}$ associated with the subdomain Ω_i for $i = 1, 2$, as

$$V^h_{m_i} = \Big\{ v^h_{m_i}(x,\mathbf{y}) = \sum_{k=1}^{m_i} \widetilde{v}^h_k\big|_{\Omega_{1D,i}}(x)\,\varphi_k(\psi_x(\mathbf{y})), \\ \text{with } \widetilde{v}^h_k \in V^h_{1D},\, x \in \Omega_{1D,i},\, \mathbf{y} \in \gamma_x \text{ and } v^h_{m_i}\big|_{\partial\Omega_i\cap(\Gamma_0\cup\Gamma_1)} = 0 \Big\},$$

and $V^h_{m_i,0} = \{v^h_{m_i} \in V^h_{m_i} : v^h_{m_i}\big|_{\gamma_\xi} = 0\}$. Moreover let $V^m_{\widehat{\gamma}_{d-1}} = span\{\varphi_k\}^m_{k=1}$ be the function space spanned by the first m modes, for any $m \in \mathbb{N}^*$.

We consider the following *relaxed Dirichlet/Neumann scheme* (see, e.g., [17, 20]). Starting from $\lambda^0 \in V^{m_1}_{\widehat{\gamma}_{d-1}} \circ \psi_\xi$, we build, for $k = 0, 1, \dots$, the sequences $\{u^{h,k}_{m_1}\}_k$, $\{u^{h,k}_{m_2}\}_k$ such that

$$u^{h,k+1}_{m_1} \in V^h_{m_1} \;:\; \begin{cases} a_1(u^{h,k+1}_{m_1}, v^h_{m_1}) = \mathcal{F}_1(v^h_{m_1}) \quad \forall v^h_{m_1} \in V^h_{m_1,0}, \\ u^{h,k+1}_{m_1}(\gamma_\xi) = \lambda^k; \end{cases} \tag{4.1}$$

$$u^{h,k+1}_{m_2} \in V^h_{m_2} \;:\; \begin{cases} a_2(u^{h,k+1}_{m_2}, v^h_{m_2}) = \mathcal{F}_2(v^h_{m_2}) \quad \forall v^h_{m_2} \in V^h_{m_2,0}, \\ a_2(u^{h,k+1}_{m_2}, R_2\mu) = \mathcal{F}_2(R_2\mu) + \mathcal{F}_1(R_1\mu) \\ \qquad\qquad - a_1(u^{h,k+1}_{m_1}, R_1\mu) \quad \forall \mu \in V^{m_2}_{\widehat{\gamma}_{d-1}} \circ \psi_\xi, \end{cases} \tag{4.2}$$

with

$$\lambda^{k+1} = \omega\, u^{h,k+1}_{m_2}\big|_{\gamma_\xi} + (1-\omega)\,\lambda^k, \tag{4.3}$$

where $a_i(\cdot,\cdot)$ and $\mathcal{F}_i(\cdot)$, for $i = 1, 2$, are the restrictions to the subdomain Ω_i of the bilinear and linear forms in (2.1), respectively, while R_i is a suitable prolongation operator from the interface γ_ξ to the whole subdomain Ω_i, with $i = 1, 2$ (see below for the definition). Here $V^{m_1}_{\widehat{\gamma}_{d-1}} \circ \psi_\xi$ is the function space spanned by the first m modes mapped back to the physical fiber γ_ξ. The update of this function is relaxed via the parameter $\omega > 0$.

The interface value λ^k as well as the weak residual on the right hand side of $(4.2)_2$ enforcing the Neumann data combine solutions involving a different number of modal functions. Therefore, suitable *matching procedures* are required. To fix the ideas, let us assume $m_1 < m_2$. We distinguish two cases:

- when we compute λ^{k+1} via the relation (4.3), we have to "reduce" the modal dimension of the solution $u^{h,k+1}_{m_2}$ since λ^{k+1} belongs to $V^{m_1}_{\widehat{\gamma}_{d-1}} \circ \psi_\xi$: the reduction is obtained simply by discarding the extra components of $u^{h,k+1}_{m_2}$. Likewise, the operator R_1 prolongates the value $\mu \in V^{m_2}_{\widehat{\gamma}_{d-1}} \circ \psi_\xi$ to Ω_1 after neglecting the last $(m_2 - m_1)$ components of μ;
- to evaluate the right hand side of $(4.2)_2$ we have to "augment" the modal dimension of the quantity $\mathcal{F}_1(R_1\mu) - a_1(u^{h,k+1}_{m_1}, R_1\mu)$ before adding it to $\mathcal{F}_2(R_2\mu)$: this is obtained by setting the $(m_2 - m_1)$ lacking components of $\mathcal{F}_1(R_1\mu) - a_1(u^{h,k+1}_{m_1}, R_1\mu)$ to zero.

REMARK 6. *The adopted matching procedure does not yield necessarily an H^1-conforming approximation $u^h_{\mathbf{m}}$. In more detail the domain decomposition scheme guarantees, up to the demanded tolerance, a continuous matching between the common modal components (corresponding to the minimum value between m_1 and m_2) and the associated fluxes. For instance, if $m_1 > m_2$ we recover the continuity of the solution also in correspondence with the remaining $(m_1 - m_2)$ modes (the last $(m_1 - m_2)$ frequency coefficients are indeed identically equal to zero for both $u^h_{m_1}$ and $u^h_{m_2}$ at the interface) whereas we do not ensure the continuity of the corresponding fluxes. If $m_1 < m_2$ we have the continuity of the fluxes but not necessarily the continuity of the frequency coefficients associated with the last $(m_2 - m_1)$ modes. As a consequence an H^1-conforming local model reduction occurs only if $m_1 > m_2$.*

From a computational viewpoint, both problems (4.1) and (4.2) lead to solve a system of coupled 1D problems in the form (3.6). The sequences $\{u^{h,k}_{m_1}\}_k$ and $\{u^{h,k}_{m_2}\}_k$ converge to the approximate solutions $u^h_{m_1}$ and $u^h_{m_2}$, respectively, provided that a suitable value for the parameter ω is chosen.

The above procedure can be generalized to boundary conditions of different type (see, e.g., [17, 20] for the details) as well as to a larger number of subdomains. In this last case, a particular attention has to be paid to the well-posedness of each subproblem. In this respect, an appropriate assignment of the interface conditions is required on each subdomain. We refer to section 4.3.3 for a practical example.

4.3. Numerical experiments. The local model reduction is assessed on three 2D test cases. The first two deal with two subdomains, while the last one involves three subdomains.

4.3.1. Test case 5. We focus on the test case used in [9] to assess the reliability of the global model reduction procedure. We solve on the rectangular domain $\Omega = (0, 2) \times (0, 1)$ a Poisson problem featuring a local heterogeneity in the source term and completed with full homogeneous Dirichlet boundary conditions. The forcing term is the characteristic function $f(x, y) = \chi_{D_1 \cup D_2 \cup D_3}(x, y)$ associated with the three circular regions $D_1 = \{(x, y) : (x - 1.5)^2 + (y - 0.5)^2 \leq 0.01\}$, $D_2 = \{(x, y) :$

$(x-0.5)^2+(y-0.25)^2 \leq 0.01\}$, and $D_3 = \{(x,y) : (x-0.5)^2+(y-0.75)^2 \leq 0.01\}$. The corresponding full solution u exhibits consequently three peaks in D_1, D_2, and D_3. Figure 4.1 displays the contour plot of u. The three peaks yield appreciable transverse features over the whole domain.

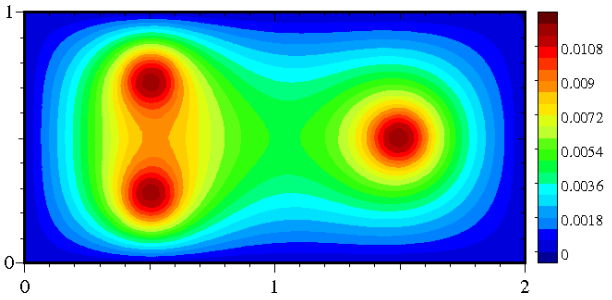

FIG. 4.1. *Test case 5: full solution.*

With a view to the local model reduction we observe that more pronounced transversal dynamics are localized in the left part of Ω (note also the steep gradients near $(0.5,0)$ and $(0.5,1)$). This suggests employing a higher number of modes in this part of the domain. The same conclusion is drawn in [9] even if in a global model reduction framework: while four modes allow us to match the full solution in correspondence with D_1, at least eight modes are required to detect the two peaks at D_2 and D_3. Thus, we resort to the domain decomposition approach upon identifying the two subdomains of Ω, $\Omega_1 = (0,1)\times(0,1)$ and $\Omega_2 = (1,2)\times(0,1)$. We apply the relaxation scheme (4.1)-(4.3) by making different choices for the modal indices m_1 and m_2. Concerning the parameters involved in such a scheme, we keep the following values, independently of the number of modes: λ^0 is the function identically equal to zero; $\omega = 0.5$; we set the convergence tolerance for the relative error to 10^{-3}; finally, the same discretization step $h = 0.02$ is used on both the domains.

We make the following three choices for the modal indices: $m_1 = 4$, $m_2 = 2$; $m_1 = 5$, $m_2 = 3$; $m_1 = 7$, $m_2 = 5$. The domain decomposition scheme converges after 2 iterations for each of these three pairs of values. Figure 4.2 illustrates the contour plots corresponding to the second iteration for the choices $m_1 = 4$, $m_2 = 2$ (top) and $m_1 = 5$, $m_2 = 3$ (bottom), while Figure 4.3 displays the reduced solution of both the iterations obtained with $m_1 = 7$ and $m_2 = 5$. Even if the behavior of the full solution is detected qualitatively in all the three cases, the choice $m_1 = 7$, $m_2 = 5$ is the only one that captures the exact solution from a quantitative viewpoint also (compare the height of the three peaks in Figures 4.2 and 4.3).

The local reduced solution $\{u_7^{0.02,2}, u_5^{0.02,2}\}$ is quantitatively in good agreement with the global reduced one $u_9^{0.02}$ proposed in [9] as a reliable approximation to the full solution in Figure 4.1. On the contrary, for $m_1 = 4$, $m_2 = 2$, the peaks are not sharply reproduced, in particular the one in correspondence with D_1 (see Figure 4.2, top). For $m_1 = 5$, $m_2 = 3$, the two peaks in Ω_1 have approximately the correct height while the one in Ω_2 is still too low (see Figure 4.2, bottom). Finally, we observe that the model discontinuity at the interface $x = 1$ turns out to be really small for all the three choices of m_1 and m_2. This discontinuity has to be ascribed to the domain decomposition algorithm since we are in the presence of a conforming local reduced solution, being $m_1 > m_2$ in all the three cases.

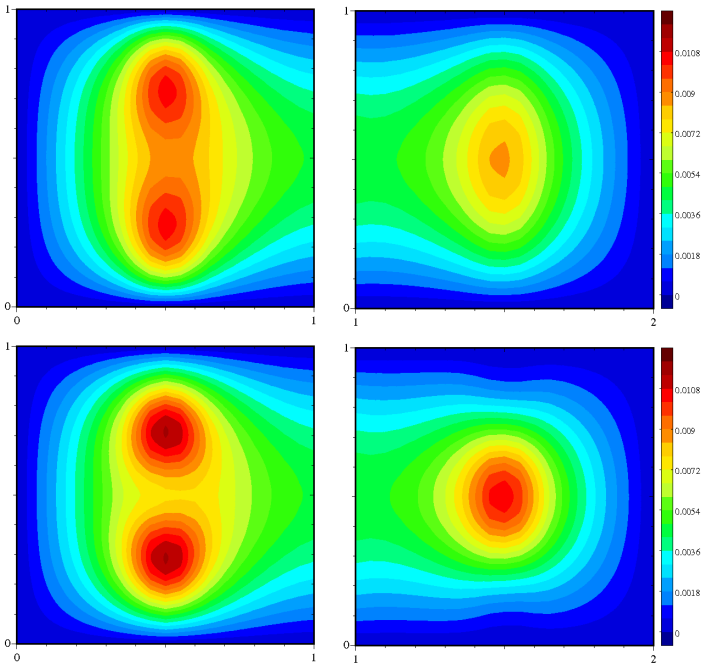

FIG. 4.2. *Local model reduction (test case 5): second iteration of the domain decomposition scheme for the choice* $m_1 = 4$, $m_2 = 2$ *(top) and* $m_1 = 5$, $m_2 = 3$ *(bottom).*

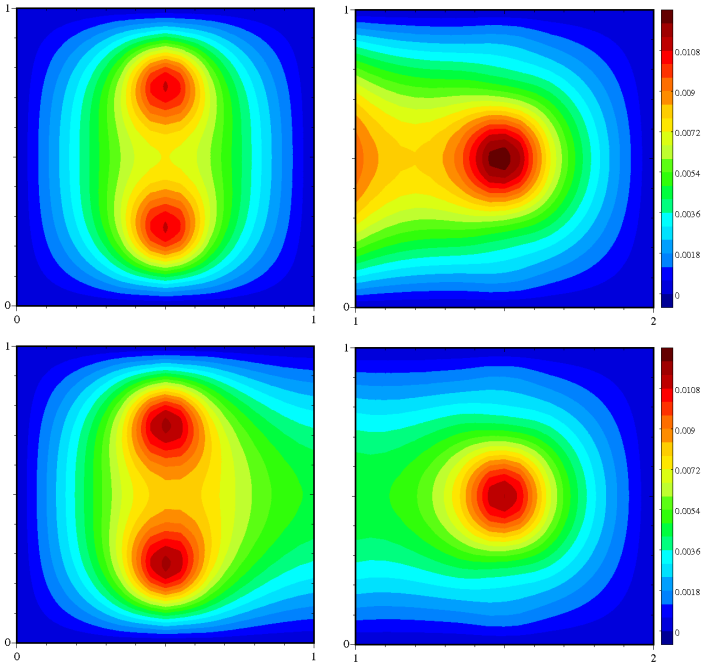

FIG. 4.3. *Local model reduction (test case 5): first (top) and second (bottom) iteration of the domain decomposition scheme for the choice* $m_1 = 7$, $m_2 = 5$.

4.3.2. Test case 6. We apply the local model reduction procedure to test case 3. Since we remarked in section 3.4.2 that few modes allow us to describe correctly the full solution u far from D while more modal functions are required on the left part of the domain, we split Ω into the subdomains Ω_1 and Ω_2 separated by the interface $\gamma_\xi = \{(\xi, y) \text{ with } \xi = 2\}$ and choose $m_1 > m_2$, i.e., conforming reduced solutions.

We make two different choices for the modal indices: $m_1 = 5$, $m_2 = 3$ and $m_1 = 7$, $m_2 = 3$. The parameters of the domain decomposition algorithm are set exactly as for test case 5, except for the discretization step h now equal to 0.05 on both Ω_1 and Ω_2. With both choices for $\{m_1, m_2\}$, the relaxation scheme converges after 4 iterations. In Figure 4.4 we show the output of the fourth iteration for $m_1 = 5$, $m_2 = 3$. A slight model discontinuity appears at the interface γ_ξ, resulting essentially from the domain decomposition algorithm. The reduced solution $\{u_5^{0.05,4}, u_3^{0.05,4}\}$ is similar to u_5^h in Figure 3.4. In particular the full solution is poorly captured in the top-left area above D. This justifies the subsequent choice $m_1 = 7$, $m_2 = 3$, resorting to an increased number of modal functions in Ω_1 only. Figure 4.5 gathers the results of the first, second, and fourth iteration associated with this choice. The third iteration is omitted since it coincides qualitatively with the last one. The area above D is now correctly described already at the second iteration. Moreover, the model discontinuity at γ_ξ is damped from the second to the fourth step of the relaxation scheme. The reduced solution $\{u_7^{0.05,4}, u_3^{0.05,4}\}$ is comparable with u_7^h (or u_9^h) in Figure 3.4. We observe that the model discontinuity does not significantly change when the difference $m_1 - m_2$ increases (compare Figure 4.4 with Figure 4.5, bottom).

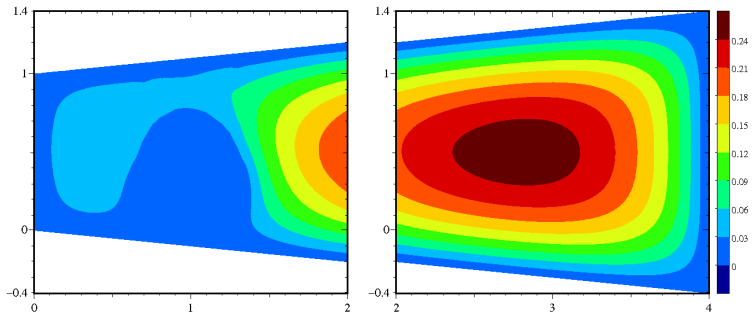

FIG. 4.4. *Local model reduction (test case 6): fourth iteration of the domain decomposition scheme for the choice $m_1 = 5$, $m_2 = 3$.*

4.3.3. Test case 7. This test case is meant to assess the local model reduction procedure in the presence of more than two subdomains. We approximate problem (3.7) on $\Omega = (0,3) \times (0,1)$ with $\mu = 1$, $\boldsymbol{\beta} = (-20, 0)^T$ (a backward field), $\sigma = 0$, and $f(x,y) = 1000\, \chi_{D_4 \cup D_5}(x,y)$, where D_4 and D_5 are the ellipsoidal regions defined by $D_4 = \big\{(x,y) \,:\, (x-1.5)^2 + 0.4\,(y-0.25)^2 \le 0.01\big\}$ and $D_5 = \big\{(x,y) \,:\, (x-1.5)^2 + 0.4\,(y-0.75)^2 \le 0.01\big\}$. Full homogeneous Dirichlet boundary conditions are enforced on $\partial\Omega$. Figure 4.6 displays the contour plot of the full solution. Owing to the strong advective field and the assigned boundary conditions, the solution is basically flat for $x > 1.7$, while it exhibits large variations in the first part of the domain with boundary layers along the lines $\{(x,0), \text{for } 0 \le x \le 1.5\}$, $\{(0,y), \text{for } 0 \le y \le 1\}$, and $\{(x,1), \text{for } 0 \le x \le 1.5\}$.

We divide Ω into three subdomains, $\Omega_1 = (0,1) \times (0,1)$, $\Omega_2 = (1,2) \times (0,1)$,

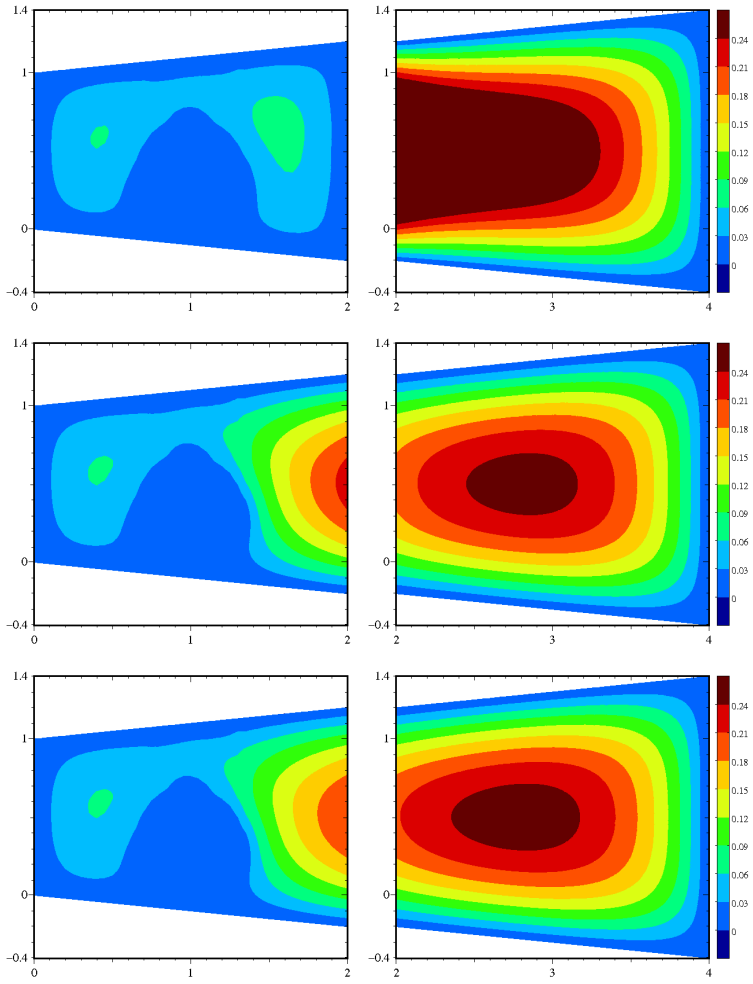

FIG. 4.5. *Local model reduction (test case 6): first (top), second (middle) and fourth (bottom) iteration of the domain decomposition scheme for the choice* $m_1 = 7$, $m_2 = 3$.

and $\Omega_3 = (2,3) \times (0,1)$, and resort to m_1, m_2, and m_3 modal functions, respectively. Algorithm (4.1)-(4.3) is thus generalized. In particular, full Dirichlet boundary conditions are assigned on $\partial\Omega_1$ (homogeneous on $\partial\Omega \cap \partial\Omega_1$ and the interface value λ_1^k along $\partial\Omega_1 \cap \partial\Omega_2$); on the other hand, on $\partial\Omega_2$ and $\partial\Omega_3$ we impose mixed boundary data (a homogeneous Dirichlet condition on $\partial\Omega_2 \cap \partial\Omega$ and $\partial\Omega_3 \cap \partial\Omega$; the interface value λ_2^k on $\partial\Omega_2 \cap \partial\Omega_3$, from the left; a Neumann condition on $\partial\Omega_1 \cap \partial\Omega_2$ and on $\partial\Omega_2 \cap \partial\Omega_3$, from the right). To run the domain decomposition algorithm we need the standard parameters twice: the initial values λ_1^0 and λ_2^0, both selected identically equal to zero; the relaxation parameters $\omega_1 = 0.5$ and $\omega_2 = 0.5$ to speed up the coupling between Ω_1 and Ω_2, and Ω_2 and Ω_3, respectively; the convergence tolerance for the relative error set to 10^{-3}.

The same discretization step h equal to 0.05 is employed in the three subdomains. This guarantees the local Péclet number to be strictly less than 1. Notice that the advective coefficient of the reduced formulation (3.9) reduces to the x-component of

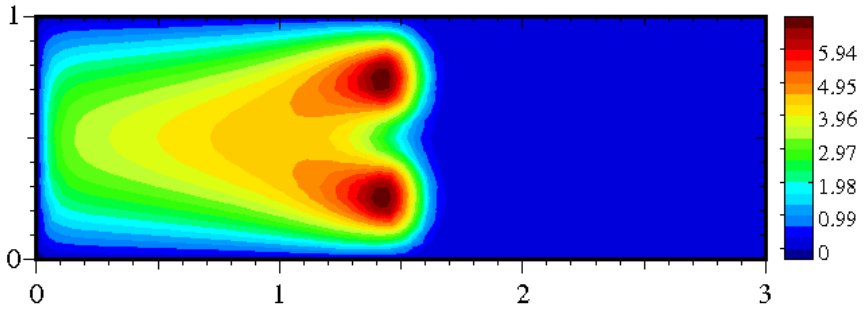

FIG. 4.6. *Test case 7: full solution.*

$\boldsymbol{\beta}$, since the quantity $\mathcal{D}_1(\mathbf{z})$ is identically 0.

The first selection for the modal indices is $m_1 = 1$, $m_2 = 3$, $m_3 = 1$. The chosen parameters lead the relaxation scheme to converge after ten iterations. Figure 5.1 collects the contour plots associated with the first, fourth, seventh, and last iteration. The full solution is reasonably well described already at the seventh step. A model discontinuity at $x = 1$ can be observed. It relaxes during the consecutive iterations, even if it can be still detected in the last reduced solution $\{u_1^{0.05,10}, u_3^{0.05,10}, u_1^{0.05,10}\}$. It can be verified that a smaller discretization step does not reduce the model jump significantly. This can be justified by the fact that the first interface is located in an area where the transverse dynamics are strongly relevant. Moreover, according to Remark 6, we are in the presence of an actual model discontinuity since $m_1 < m_2$. On the contrary, no model discontinuity appears around $x = 2$ where the solution is completely flat and since $m_2 > m_3$.

To improve the quality of the reduced solution we have assessed a second (richer) choice for the modal indices, namely $m_1 = 3$, $m_2 = 5$, $m_3 = 1$. We preserve the values above for the parameters of the relaxation scheme. Convergence is reached again after ten steps. By comparing the corresponding contour plots in Figures 5.1 and 5.2, we recognize a significant improvement in terms of model discontinuity. It is clearly damped in the presence of the richer modal basis expansion. A low sensitivity with respect to the choice made for h is observed also in this case.

This example highlights the importance of the position of the interface between two adjacent subdomains for the effectiveness of the present approach. An automatic collocation of such an interface driven by some a posteriori estimation is currently under investigation ([16]).

5. Conclusions and perspectives. We have proposed a *hierarchical model reduction* procedure to deal with problems characterized by a main stream direction (from blood to river flows, or internal combustion engines) with possible local transverse perturbations. The dominant direction is reflected by the computational domain at hand, which can be identified with a fiber bundle aligned with the main stream itself.

The key-idea is to derive a hierarchy of 1D reduced models; the simplest one coincides with a purely 1D problem associated with the leading direction. By hierarchically enriching it via suitable modal functions, we obtain more accurate reduced models that better capture the transverse dynamics of the problem at hand. Independently of the spatial dimension where the full problem is posed, the reduced

formulation leads to a system of 1D problems associated with the main stream and coupled by the transverse dynamics. The system size depends on the number of modal functions. Consequently, computational saving with respect to the solution of the full problem is expected when few modes are switched on along the transverse directions and, especially, in the context of 3D applications.

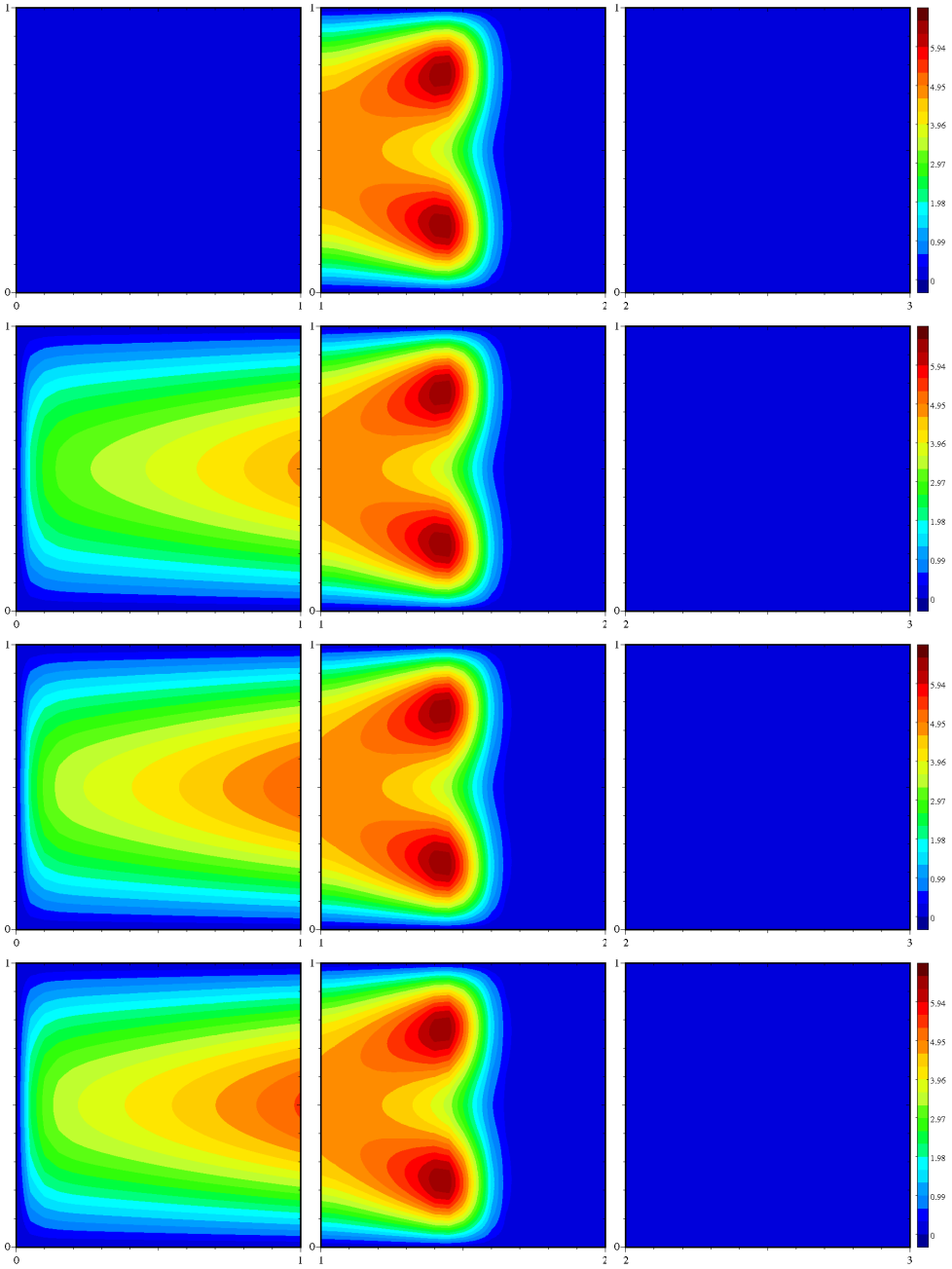

FIG. 5.1. *Local model reduction (test case 7): first, fourth, seventh, and tenth iteration (top-bottom) of the domain decomposition scheme for the choice* $m_1 = 1$, $m_2 = 3$, $m_3 = 1$.

The hierarchical model reduction procedure provides an alternative approach to the geometrical multiscale approach (see, e.g., [11, Chap. 11]), where models with a different dimension (for instance, 1D with 2D or 3D) are coupled. Both approaches resort to a domain splitting matching the different solutions. However, the domain decomposition associated with the hierarchical reduction yields an easier and faster

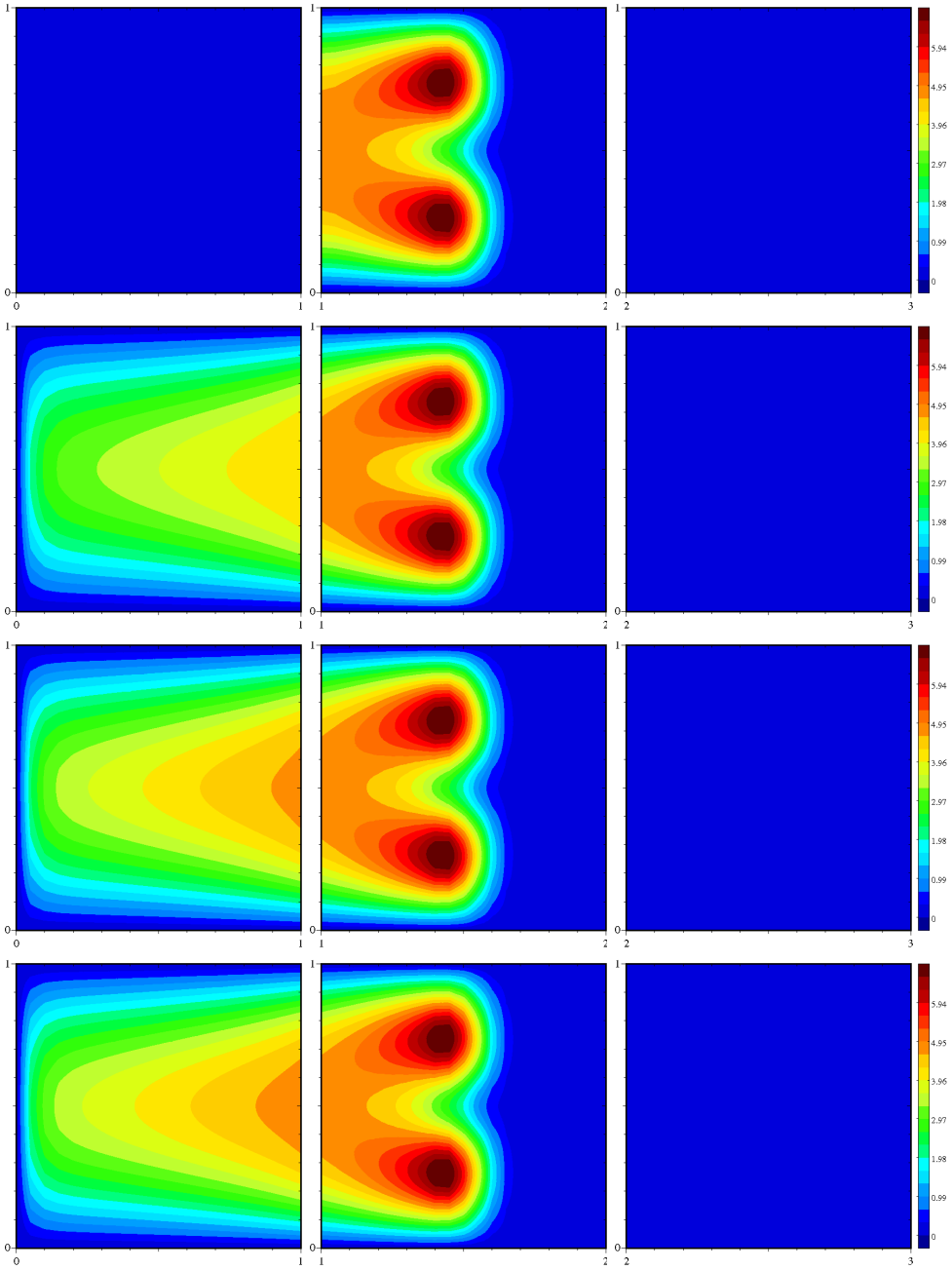

FIG. 5.2. *Local model reduction (test case 7): first, fourth, seventh, and tenth iteration (top-bottom) of the domain decomposition scheme for the choice* $m_1 = 3$, $m_2 = 5$, $m_3 = 1$.

relaxation scheme compared with the geometrical multiscale approach.

Many important aspects deserve further investigation. First of all, the set-up of a modeling adaptive procedure to automatically associate different modal indices with different parts of the domain according to the local heterogeneities of the problem at hand. This goal is pursued in the second part of this paper [16]. We refer, e.g., to [1, 3, 23] for an a posteriori error analysis in the context of thin domains, and to [19]. A second issue is to generalize the hierarchical model reduction procedure to more complex problems (e.g., Oseen or Navier-Stokes equations).

Acknowledgments. This work has been partially supported by the COFIN2006 Project: "*Numerical Approximation of Multiscale and Multiphysic Problems with Adaptive Techniques*".

REFERENCES

[1] M. Ainsworth, *A posteriori error estimation for fully discrete hierarchic models of elliptic boundary value problems on thin domains*, Numer. Math., 80 (1998), pp. 325–362.

[2] M. Amara, D. Capatina, and D. Trujillo, *Hydrodynamical modelling and multidimensional approximation of estuarian river flows*, Seventh Zaragoza-Pau Conference on Applied Mathematics and Statistics (Spanish) (Jaca, 2001), Monogr. Semin. Mat. García Galdeano, 27 (2003), pp. 41–48, Univ. Zaragoza, Zaragoza.

[3] I. Babuška and Ch. Schwab, *A posteriori error estimation for hierarchic models of elliptic boundary value problems on thin domains*, SIAM J. Numer. Anal., 33 (1996), pp. 221–246.

[4] B.J. Bellhouse, F.H. Bellhouse, C.M. Curl, T.I. MacMillan, A.J. Gunning, E.H. Spratt, S.B. MacMurray and J.M. Nelems, *A high efficiency membrane oxygenator and pulsatile pumping system and its application to animal trials*, Trans. Amer. Soc. Artif. Int. Organs, 19 (1973), pp. 72–79.

[5] C. Canuto, M. Y. Hussaini, A. Quarteroni and T. A. Zang, *Spectral Methods. Fundamentals in Single Domains*, Springer-Verlag, Berlin Heidelberg, 2006.

[6] C. Canuto, Y. Maday and A. Quarteroni, *Analysis of the combined finite element and Fourier interpolation*, Numer. Math., 39 (1982), pp. 205–220.

[7] C. Canuto, Y. Maday and A. Quarteroni, *Combined finite element and spectral approximation of the Navier-Stokes equations*, Numer. Math., 44 (1984), pp. 201–217.

[8] I. Daubechies, *Ten Lectures on Wavelets*, Society for Industrial and Applied Mathematics (SIAM), Philadelphia, 1992.

[9] A. Ern, S. Perotto and A. Veneziani, *Hierarchical model reduction for advection-diffusion-reaction problems*, in *Numerical Mathematics and Advanced Applications*, K. Kunisch, G. Of, O. Steinbach Eds., Springer-Verlag, Berlin Heidelberg, 2008, pp. 703–710.

[10] L. Formaggia, F. Nobile, A. Quarteroni and A. Veneziani, *Multiscale modelling of the circulatory system: a preliminary analysis*, Comput. Visual. Sci., 2 (1999), pp. 75–83.

[11] L. Formaggia, A. Quarteroni and A. Veneziani (eds.), *Cardiovascular Mathematics*, Series: Modeling Simulation and Applications, Vol. 1, Springer, 2009.

[12] P. Grisvard, *Equations différentielles abstraites*, Ann. Sci. Ecole Norm. Sup., 4 (1969), pp. 311–395.

[13] B. Heinrich, *The Fourier finite element method for Poisson's equation in axisymmetric domains with edges*, SIAM J. Numer. Anal., 33 (1996), pp. 1885–1911.

[14] J.L. Lions and E. Magenes, *Non Homogeneous Boundary Value Problems and Applications*, Springer, Berlin-Heidelberg-New York, 1972.

[15] E. Miglio, S. Perotto and F. Saleri, *Model coupling techniques for free-surface flow problems. Part I*, Nonlinear Analysis, 63 (2005), pp. 1885–1896.

[16] S. Perotto and A. Ern, *Hierarchical local model reduction for elliptic problems II: an a posteriori error estimator*, in preparation, (2009).

[17] A. Quarteroni and A. Valli, *Domain Decomposition Methods for Partial Differential Equations*, Numerical Mathematics and Scientific Computation, Oxford University Press, New York, 1999.

[18] A. Quarteroni and A. Veneziani, *Analysis of a geometrical multiscale model based on the coupling of ODEs and PDEs for blood flow simulations*, Multiscale Model Simul., 1 (2003), pp. 173–195.

[19] E. Stein, M. Rüter and S. Ohnimus, *Error-controlled adaptive goal-oriented modeling and finite element approximations in elasticity*, Comput. Methods Appl. Mech. Engrg., 196 (2007), pp. 3598–3613.
[20] A. Toselli and O. Widlund, *Domain Decomposition Methods–Algorithms and Theory*, Springer-Verlag, Berlin Heidelberg, 2005.
[21] M. Vogelius and I. Babuška, *On a dimensional reduction method. I. The optimal selection of basis functions*, Math. Comp., 37 (1981), pp. 31–46.
[22] ———, *On a dimensional reduction method. II. Some approximation-theoretic results*, Math. Comp., 37 (1981), pp. 47–68.
[23] ———, *On a dimensional reduction method. III. A posteriori error estimation and an adaptive approach*, Math. Comp., 37 (1981), pp. 361–384.
[24] C.B. Vreugdenhil, *Numerical Methods for Shallow–Water Flows*, Kluwer Academic Press, Dordrecht, 1998.